HHS Public Access

Author manuscript

Neuron. Author manuscript; available in PMC 2019 December 05.

Published in final edited form as:

Neuron. 2018 December 05; 100(5): 1083–1096.e5. doi:10.1016/j.neuron.2018.10.016.

FOXG1 orchestrates neocortical organization and cortico-cortical connections

Francesca Cargnin[1], **Ji-Sun Kwon**[1], **Sol Katzman**[4], **Bin Chen**[3], **Jae W. Lee**[1], and **Soo-Kyung Lee**[1,2,5,*]

[1]Papé Family Pediatric Research Institute, Department of Pediatrics, Oregon Health & Science University, Portland, OR 97239, USA

[2]Vollum Institute, Oregon Health & Science University, Portland, OR 97239, USA

[3]Department of Molecular, Cell and Developmental Biology, University of California, Santa Cruz, Santa Cruz, CA 95064, USA

[4]Genomics Institute, University of California, Santa Cruz, Santa Cruz, CA 95064, USA

[5]Lead Contact

SUMMARY

The hallmarks of FOXG1 syndrome, which results from mutations in a single *FOXG1* allele, include cortical atrophy and corpus callosum agenesis. However, the etiology for these structural deficits and the role of FOXG1 in cortical projection neurons remain unclear. Here we demonstrate that Foxg1 in pyramidal neurons plays essential roles in establishing cortical layers and the identity and axon trajectory of callosal projection neurons. The neuron-specific actions of Foxg1 are achieved by forming a transcription complex with Rp58. The Foxg1-Rp58 complex directly binds and represses *Robo1, Slit3*, and *Reelin* genes, the key regulators of callosal axon guidance and neuronal migration. We also found that inactivation of one *Foxg1* allele specifically in cortical neurons was sufficient to cause cerebral cortical hypoplasia and corpus callosum agenesis. Together, this study reveals a novel gene regulatory pathway that specifies neuronal characteristics during cerebral cortex development and sheds light on the etiology of FOXG1 syndrome.

eTOC Paragraph

Cargnin et al. report essential roles of FOXG1 transcription factor in building the functional cerebral cortex. This study sheds light on the disease mechanism of human disorder FOXG1 syndrome.

*Correspondence: leesoo@ohsu.edu.

AUTHOR CONTRIBUTIONS

Conceptualization, F.C. and S.L; Methodology, F.C. and S.L; Investigation, F.C. and S.L; Formal Analysis, F.C. and J.K.; Resources, S.K. and B.C.; Writing - Original Draft, F.C. and S.L; Writing - Review & Editing, F.C., J.W.L. and S.L; Visualization, F.C.; Supervision, J.W.L. and S.L; Funding Acquisition, B.C., J.W.L. and S.L.

DECLATION OF INTERESTS

The authors declare no competing interests.

Keywords

Foxg1; BF1; Rp58; Znf238; Zbtb18; radial migration; callosal projection; corpus callosum; transcription factor; cortex; development

INTRODUCTION

Building a functional brain requires intricate gene regulation. An excellent example of this is the six-layered mammalian cerebral cortex that is generated in an inside-out fashion. This cytoarchitecture of the cerebral cortex is critical for its function to control higher-order cognitive behaviors, sensory perception, and consciousness. In the developing cortex, neural progenitors actively proliferate in the germinal zone, and then sequentially produce diverse types of excitatory projection neurons, which establish the cortical plate (CP) (Greig et al., 2013). Early-born neurons occupy deep cortical layers (layers 5/6), and late-born neurons migrate past them to settle in upper layers (layers 2/3/4). The timely migration and positioning of neurons within the CP are essential for the emergence of proper neuronal identity and function. Among distinct types of cortical projection neurons, callosal projection neurons (CPNs), which reside primarily in upper layers, play a vital role in coordinating information between the cerebral hemispheres as their axons form the corpus callosum connecting the two hemispheres. Importantly, corpus callosum agenesis, which encompasses complete or partial absence of the corpus callosum, has been found in various neurodevelopmental and psychiatric disorders (Paul et al., 2007). The positioning and axon navigation of CPNs are regulated by a complex interplay of multiple guidance genes such as Robo and Slit (Lindwall et al., 2007). Numerous studies have established that the correct expression patterns of proneural and guidance molecules in the developing cerebral cortex are critical for the formation of brain architecture and interhemispheric connectivity. However, the transcriptional regulatory mechanism that establishes the dynamic expression patterns of proneural and guidance genes and how the dysregulation of this process contributes to human disorders remain ambiguous.

Recent progress in genetic testing technology has facilitated discovery of haploinsufficiency of multiple genes associated with human neurodevelopmental disorders, including *FOXG1* (also known as *Brain Factor 1*) and *RP58* (also known as *ZNF238*, *ZFP238* or *ZBTB18*). Deletions or mutations in a single allele of the transcription factor gene *FOXG1* cause FOXG1 syndrome (initially known as atypical Rett syndrome), which is characterized by developmental delay, severe intellectual disability, epilepsy, absent language, and dyskinesis (Florian et al., 2012; Kortum et al., 2011). Two hallmarks of FOXG1 syndrome are cortical atrophy and characteristic agenesis of the corpus callosum. Notably, hemizygous deletions or mutations in another transcription factor *RP58* have also been found in patients with intellectual disability, absent language, microcephaly and corpus callosum agenesis (de Munnik et al., 2014; Perlman et al., 2013; van Bon et al., 2008) or atypical Rett syndrome (Lopes et al., 2016). These data suggest that the architecture of the human cerebral cortex is highly sensitive to *FOXG1* and *RP58* gene dosage.

FOXG1, a member of the forkhead transcription factor family, is one of the earliest transcription factors whose expression is induced specifically in the neural progenitors of the forebrain (Tao and Lai, 1992). Complete elimination of *Foxg1* in mice leads to a drastic reduction of the cerebral hemispheres due to reduced proliferation and precocious differentiation of Foxg1-deficient neural progenitors (Hanashima et al., 2002; Xuan et al., 1995). Although the downregulation of Foxg1 in pyramidal neuron precursors is important for their differentiation to immature neurons, interestingly, Foxg1 expression is later re-induced in maturing neurons at the upper intermediate zone (IZ), in which it promotes the acquisition of bipolar morphology of neurons and their entry into the CP (Miyoshi and Fishell, 2012). Afterward, Foxg1 remains highly expressed in postmigratory neurons in the CP, but the role of Foxg1 in this context remains unclear.

The decisive actions of Foxg1 in neural progenitors, along with severe human conditions resulting from a loss of one copy of *FOXG1*, raise important questions. First, does Foxg1 play any roles in pyramidal neurons within the CP? Second, what are the molecular mechanisms by which Foxg1 exerts disparate actions at different time points in the developing cerebral cortex? Last but not least, what is the mechanistic basis underlying cortical hypoplasia and profound corpus callosum hypogenesis in FOXG1 syndrome?

In this study, we demonstrate that Foxg1 action in post-mitotic neurons is imperative to generate the cortical laminar structure in an inside-out fashion and to form the corpus callosum. Our analyses of chromatin immunoprecipitation followed by sequencing (ChIPseq) revealed that Foxg1 forms a transcription repressive complex with Rp58, which directs callosal projections and promotes the radial migration of cortical neurons. Further, our analyses revealed the novel target genes of Foxg1, Robo1 and Slit3, which are critical for guiding callosal axons to cross the midline. Our data indicate that the co-regulation of CPN identity and callosal projections by Foxg1 is a crucial element responsible for establishing cortico-cortical projections. Furthermore, our study provides key insights into the molecular basis of cortical atrophy and corpus callosum agenesis in human FOXG1 syndrome.

RESULTS

Foxg1 action in post-mitotic neurons is required for the cortical laminar organization and corpus callosum formation

Foxg1 is upregulated in cortical neurons migrating into the CP and remains highly expressed in post-migratory projection neurons within the CP (Miyoshi and Fishell, 2012) (Figure S1B). To investigate the role of Foxg1 in cortical pyramidal neurons, we inactivated the *Foxg1* gene using *NEX-Cre* (Goebbels et al., 2006), and analyzed both *Foxg1*-conditional null (*Foxg1* $^{fi/fi}$*;NEX-Cre, Foxg1-cKO*) and *Foxg1*-conditional het (*Foxg1*$^{fi/+}$*;NEX-Cre, Foxg1-cHET*) mice in parallel with their littermate controls (*Foxg1* $^{fi/fi}$, control). The *Foxg1* floxed (*Foxg1*^{fi}) allele expresses Flpe recombinase upon CREmediated *Foxg1* deletion, resulting in GFP expression in *Foxg1*-deleted cells when a Flpe-dependent GFP reporter line (*R26R-CAG-FRTstop-eGFP, RCE*) is integrated (Miyoshi and Fishell, 2012). Thus, our mouse scheme enables GFP expression only when *NEX-Cre*-mediated recombination occurs in Foxg1-expressing cells (Figure S1A). Cre, Flp and GFP were highly expressed in the

cortical neurons, whereas their expression was largely excluded from $Pax6^+$ radial glial progenitors or $Tbr2^+$ intermediate progenitors in *Foxg1-cKO* and *Foxg1-cHET* cortices (Figure S1B,C,E). Confirming that GFP expression indicates the inactivation of Foxg1, Foxg1 expression was eliminated in the prospective CP of *Foxg1-cKO* mice and significantly reduced in the CP of *Foxg1-cHET* compared to control, but it still remained in in the VZ or subventricular zone (SVZ) (Figure S1B,C). As NEX-Cre activity was observed in a subset of mitotic progenitors when a highly sensitive viral reporter was used (Wu et al., 2005), we tested if the progenitors decrease by deletion of *Foxg1* by NEX-Cre, similar to global *Foxg1* mutants (Hanashima et al., 2002; Siegenthaler et al., 2008). $Pax6^+$ or $Tbr2^+$ progenitors did not show a significant change in their numbers in *Foxg1-cKO* or *Foxg1-cHET* cortices, consistent with the absence of GFP, an indicator of Foxg1 inactivation, in the progenitor zone (Figure S1B–E). Together, these data indicate that Foxg1 action is inactivated in cortical neurons while Foxg1 expression is largely maintained in progenitors in *Foxg1-cKO* and *Foxg1-cHET* cortices.

In *Foxg1-cKO* brains, the cortex was substantially thinner, the ventricle was enlarged, and the intermediate zone (IZ) was not well-defined at P0 (Figure 1A). Furthermore, the corpus callosum was missing throughout the anterior-posterior axis, and the hippocampus failed to develop in *Foxg1-cKO* mice (Figure 1A). In *Foxg1-cHET* brains, in which the *Foxg1* dosage was lowered in post-mitotic neurons, the corpus callosum was longitudinally shorter and the hippocampus was hypoplastic (Figure 1A). Notably, the global *Foxg1* heterozygous (*HET*, +/−) mice, which mimic the genotype of human FOXG1 syndrome patients, also exhibited the hypogenesis of the corpus callosum and hippocampus (Figure S2A). Our data demonstrate that the action of Foxg1 in cortical neurons is required for the formation of cortical laminar structure, corpus callosum, and hippocampus. Given that the corpus callosum hypogenesis and hippocampus atrophy are common features among human FOXG1 syndrome brains, and global *HET* and *Foxg1-cHET* mouse brains (Eagleson et al., 2007; Florian et al., 2012; Kortum et al., 2011; Shen et al., 2006; Siegenthaler and Miller, 2008), the haploinsufficiency of Foxg1 action in post-mitotic neurons is likely to be a main contributing factor to the malformation of the cortex and hippocampus in the FOXG1 syndrome.

Foxg1 plays a critical role for the cortical layer formation

The prominent phenotypes in *Foxg1-cKO* and *cHET* cortices led us to investigate if the Foxg1 activity in cortical pyramidal neurons is needed for the generation of cortical layers. In E16.5 *Foxg1-cKO* cortices, the neuronal cell body-dense CP area was not evident, and $Tbr1^+$ and $Ctip2^+$ deep layer neurons were broadly dispersed from the IZ close to the pial surface, and the Ctip2 level decreased (Figure 1B). In P0 *Foxg1*-cKO cortices, $Cux1^+$ upper layer neurons, $Satb2^+$ CPNs, and Satb2 expression levels were markedly reduced, while $Tbr1^+$ neurons increased (Figure 1C). Interestingly, the remaining low-level $Stat2^+$ neurons were located below $Tbr1^+/Ctip2^+$ neurons in *Foxg1*cKO cortices (Figure 1C), suggesting that the cortical layers are reversed in the absence of Foxg1.

Notably, both *Foxg1-cHET* and global *HET* mice exhibited a significant reduction of Satb2$^+$ and Cux1$^+$ upper layer neurons (Figure 1C,D, S2B–E), suggesting that the timely production of CPNs and upper layer neurons requires a full *Foxg1* gene dosage.

Together, our data indicate that the action of Foxg1 in cortical pyramidal neurons is critical for the orderly formation and maintenance of the cortical laminar structure. Interestingly, the loss of a single copy of *Foxg1* was sufficient to reduce CPNs, suggesting that upper layer neurons are vulnerable to the reduced *Foxg1* dosage.

Haploinsufficiency of *Foxg1* in controlling axonal navigation of CPNs

Next, we tested if the *Foxg1* gene dosage also influences axon projection of CPNs, a critical characteristic of CPNs that is needed to connect the two hemispheres, using the axonal marker L1. In *Foxg1-cKO* mice, GFP-positive L1$^+$ axons of cortical neurons failed to cross the midline and accumulated close to the midline at E16.5 and P0 (Figure 2A,B,E). In addition, in *Foxg1-cKO* cortices, GFP-negative L1$^+$ thalamocortical axons were misrouted and invaded the CP (*arrow*, Figure 2C) and formed the aberrant bundle close to the pial surface (*arrowhead*, Figure 2C). Neuropilin-1$^+$ neurons that send pioneer axons were present in the cingulate cortex but the overall level of Neuropilin-1 reduced in *Foxg1-cKO* brains (Figure S2G). These results indicate that the removal of Foxg1 in cortical pyramidal neurons is sufficient to produce marked deficits in the formation of the callosal axonal tract, underscoring a critical role of Foxg1 in cortical neurons.

Interestingly, *Foxg1-cHET* mice showed a remarkable reduction in callosal axon tract crossing the midline at E16.5 (Figure 2A), while Neuropilin-1 expression was comparable between *Foxg1-cHET* and control mice (Figure S3A). In P0 *Foxg1-cHet* brains, a substantial fraction of L1$^+$/GFP$^+$ callosal axons were stalled at the midline and formed the Probst bundle (*arrowheads*, Figure 2B). To further investigate callosal axon defects in *Foxg1-cHET* mice, we performed axonal tracing experiments by injecting DiI, a lipophilic membrane staining dye, into the superficial cortex of one hemisphere of P7 mice. We then examined the interhemispheric projection pattern to the contralateral hemisphere by monitoring DiI diffusion. In *Foxg1-cHET* brains, a substantial fraction of callosal axons stalled and formed Probst bundles at the midline (*arrowhead*, Figure 2D), and the amount of callosal axonal bundles passing through the midline was reduced compared to control littermates (Figure 2D,E). Moreover, some callosal axons took an aberrant turn to the ventral side around the midline and projected toward the septum (*star*, Figure 2D). The global *Het* brains also exhibited deficits in callosal axonal projections that are remarkably similar to *Foxg1-cHET* mice (Figure S2F). Together, it is evident that the full dosage of the *Foxg1* gene in cortical neurons is required to establish cortico-cortical projections, providing novel mechanistic insights into corpus callosum anomalies in the FOXG1 syndrome.

As the midline glia play an important role in establishing callosal projections (Unni et al., 2012), we examined if the midline structure is disturbed in *Foxg1-cHET* and *Foxg1-cKO* brains using the glial marker GFAP. GFAP$^+$ astroglia did not express GFP in *Foxg1* conditional mutants (Figure S2H), indicating that Foxg1 was not inactivated in their midline glia. Despite the lack of GFP expression in the midline glia, however, indusium griseum astroglia exhibited developmental defects in both *Foxg1-cHET* and *Foxg1-cKO*, while the

glial wedge formed relatively normally. During development, the indusium griseum glia emerge from the VZ and migrate to the pial surface, in which they retract their radial process and form the indusium griseum (Smith et al., 2006). In *Foxg1-cKO* brains, the indusium griseum glia were displaced ventrally and located below the glial wedge (Figure S2H). Interestingly, in both *Foxg1-cHET* and global *Het* brains, the indusium griseum glia failed to retract the radial processes, resulting in the underdeveloped structure (Figure S2H,I). Our data suggest that the loss of Foxg1 action in neurons leads to the midline glia deficits

Foxg1 functions cell-autonomously to control the laminar position and axon trajectory of upper layer neurons

The marked deficits in the generation of CPNs and inter-cortical connection in *Foxg1cKO* and *cHET* brains raised the possibility that radial migration and axon targeting of late-born neurons requires *Foxg1* full dosage and, therefore, was perturbed by reduced *Foxg1* levels. To test this possibility, we labeled a subset of late-born neurons in cortices of *Foxg1-cKO, cHET* and control mice with tdTomato using *in utero* electroporation of E15.5 embryos, and monitored the migratory and axon trajectory pattern of tdTomato$^+$ neurons at P0 and P7. Strikingly, in *Foxg1-cKO* cortices, the lateborn neurons failed to radially migrate through the early-born neurons and accrued below the early-born neurons (Figure 3A), suggesting that the failed radial migration of *Foxg1*-deficient late-born neurons resulted in the reversed pattern of cortical layers (Figure 1C). In *Foxg1-cHET* cortices, the radial migration of late-born neurons was substantially delayed compared to controls (Figure 3A,B). At P0, ~67% of tdTomato$^+$ neurons reached layers 2/3 in control cortices, whereas only ~18% of tdTomato$^+$ neurons were found in layers 2/3 and a significantly increased number of tdTomato$^+$ neurons still remained in deep layers 5/6 and the IZ in *Foxg1-cHET* cortices. By P7, most tdTomato$^+$ neurons entered the CP and position themselves in the upper layers in *Foxg1-cHET* mice (Figure 3C). Interestingly, however, the callosal axons of this group of late-born neurons in *Foxg1-cHET* cortices were defasciculated most noticeably at the midline, unlike the callosal axons in control cortices that formed the tight bundle (Figure 3D). The delayed radial migration of the late-born neurons was also observed in global *HET* cortices (Figure S3). Together, our results demonstrate that Foxg1 action in cortical projection neurons is crucial in forming the correct inside-out pattern of cortical layers. Our data also show that the loss of a single functional allele of *Foxg1* results in a slower integration of neurons into the upper cortical layer and the defasciculation of callosal axonal tracts.

To test if Foxg1 acts cell-autonomously to promote radial migration and tight axon tract formation at the midline in a dosage-sensitive manner, we employed the experimental scheme that allowed us to evaluate the motility and axon projection of *Foxg1-HET* neurons in the context of a Foxg1 full dosage cellular background. We electroporated E15.5 cortices of *Foxg1$^{fi/+}$;RCE* embryos with either CRE-T2A-tdTomato or tdTomato expression vector *in utero* and monitored the behavior of tdTomato$^+$ transfected cells at P0 or P7. In this scheme, only *Foxg1-HET* cells express GFP upon CRE-mediated deletion of a copy of *Foxg1*. The radial migration of *Foxg1-HET* neurons was significantly delayed relative to that of control neurons, as demonstrated by a lower proportion of *Foxg1-HET* neurons reached in layers 2/3 compared to control neurons (Figure 3E,F). Furthermore, the axons of *Foxg1-HET* neurons crossing the midline failed to form the tight bundle (Figure 3G).

Our results suggest that Foxg1 controls the timely integration of cortical pyramidal neurons to the upper layers and the navigation of callosal axons in cellautonomous and Foxg1 dosage-sensitive manners.

ChIPseq analyses revealed Foxg1 collaborates with RP58 in cortical neurons

Our studies suggest that the Foxg1 action in cortical pyramidal neurons is crucial for coordinating laminar position and axon trajectory in the cortex, which is distinct from its role in neural progenitors as a regulator of patterning, cell cycle, and progenitor identity (Hanashima et al., 2002; Hardcastle and Papalopulu, 2000; Martynoga et al., 2005; Seoane et al., 2004; Xuan et al., 1995). The role of Foxg1 in controlling axon trajectory in the forebrain was previously unknown. How does Foxg1 exert these disparate actions in a cell context-dependent manner? We considered the possibility that in cortical neurons Foxg1 recognizes and binds to specific target loci by forming a neuron-specific complex with other partner transcription factors. To test this idea, we identified gene regulatory sequences occupied by Foxg1 using ChIPseq analyses in E15.5 cortices, within which Foxg1 is highly expressed in neurons entering to the CP and postmigratory neurons within the CP. Our ChIPseq analyses revealed genomic regions that recruit Foxg1 in embryonic cortices (Table S 1). To search for transcription factors that are co-recruited with Foxg1 to these genomic loci, we performed motif analyses on Foxg1-bound ChIPseq peaks (Figure 4A). As predicted, the most strongly enriched motif was the Foxg1-binding site. Interestingly, the motif enriched with the second highest significance was the binding site for Rp58. We found that 3256 Foxg1-bound genomic loci possess both Foxg1 and Rp58 motifs within 200 base pair (bp) from the summit of the peak (Figure 4B, Table S2). The plotting of the position of Foxg1 and Rp58 motifs relative to the peak summit (position 0 in the graphs of Figure 4B) revealed that both Foxg1 and Rp58 motifs were enriched in the proximity of the peak summit in these 3256 peaks. These data raise the possibility that Foxg1 and Rp58 are co-recruited as a complex to these Foxg1/Rp58 motifs-containing target loci (Figure 4F). Supporting this possibility, both Foxg1 and Rp58 are upregulated in neurons that begin to enter into the CP, and both are highly co-expressed in postmigratory pyramidal neurons in the CP (Figure 4C, S4A). Rp58 was still expressed in the presumptive CP in *Foxg1-cKO* and *cHET* mice (Figure 4C,D), suggesting that Rp58 expression in cortical neurons is not dependent on Foxg1 action. Endogenous Foxg1 and Rp58 were co-immunopurified in E15.5 cortices (Figure 4E), indicating that Foxg1 associates with Rp58 in cortical pyramidal neurons. Similarly, Foxg1 interacted with Rp58 in HEK293 cells transfected with Foxg1- and Rp58-expression vectors (Figure S4B). Overall, our genome-wide studies indicate that Foxg1 and Rp58 form a complex and control transcription of common target genes in cortical pyramidal neurons during cortex development (Figure 4F).

Foxg1-Rp58 complex regulates genes involved in neuronal migration and axon navigation

Loss-of-function mutations in *Foxg1* and *Rp58* exhibit highly similar phenotypes in both mice and human. *Rp58*-null mice show microcephaly, axon misprojection, and corpus callosum agenesis (Okado et al., 2009; Xiang et al., 2012). The misprojection of thalamocortical axons toward the pial surface of the cortex is strikingly similar between *Rp58*-null cortices (Okado et al., 2009) and *Foxg1-cKO* cortices (Figure 2C). Human patients with deletions or mutations in *RP58* present with intellectual disability,

microcephaly and corpus callosum agenesis (de Munnik et al., 2014; Lopes et al., 2016; Perlman et al., 2013; van Bon et al., 2008), like FOXG1 syndrome patients. The remarkable phenotypic similarity between *Foxg1* and *Rp58* mutants, combined with our finding that Foxg1 and Rp58 form a complex in the CP (Figure 4), led us to hypothesize that Foxg1-Rp58 regulate a subset of Foxg1 target genes that mediate Foxg1 action in cortical projection neurons. The 3256 ChIPseq peaks containing both Foxg1- and Rp58binding motifs were annotated to 2246 genes (Figure 4B, Table S2), providing a set of potential target genes of the Foxg1-Rp58 complex. Interestingly, the 2246 putative target genes of Foxg1-Rp58 are significantly enriched for the categories of cell adhesion, cell morphogenesis, neuron projection and axonogenesis (Figure 5A, Table S3). These analyses suggest that the Foxg1-Rp58 complex regulates genes controlling neuronal migration and projection.

Notably, the Foxg1/Rp58 motifs-containing peaks were found in the intron of *Robo1* and *Slit3* genes as well as *Reelin* (Figure 5B). Robo-Slit signaling is a key regulator of projection and fasciculation of axons crossing the midline (Andrews et al., 2006; Bagri et al., 2002; Devine and Key, 2008; Lindwall et al., 2007). Reelin plays a critical role in controlling radial migration of cortical neurons (Franco et al., 2011; Hashimoto-Torii et al., 2008; Jossin and Cooper, 2011). To test whether the Foxg1Rp58 complex is recruited to the ChIPseq peaks in the *Robo1, Slit3,* and *Reelin* genes *in vivo* and whether this recruitment is affected by the loss of *Foxg1*, we performed ChIP assays with Foxg1 and Rp58 antibodies in E15.5 *Foxg1-cKO, Foxg1-cHET* and control cortices and quantified the occupancy of Foxg1 and Rp58 on the putative Foxg1-Rp58binding sites. Both Foxg1 and Rp58 bound to each of Foxg1-bound ChIPseq peaks in control cortices (Figure 5C), supporting the idea that Foxg1 and Rp58 are co-recruited to *Robo1, Slit3,* and *Reelin* as a complex (Figure 5D). Foxg1-binding to its target genes significantly reduced in *Foxg1-cHET* and further decreased in *Foxg1-cKO,* compared to control cortices (Figure 5C). Interestingly, the recruitment of Rp58 to the Foxg1-Rp58 target loci also significantly decreased in *Foxg1-cHET* and *Foxg1-cKO* brains, relative to control brains (Figure 5C), despite comparable Rp58 levels among *Foxg1-cKO*, *Foxg1cHET* and control cortices (Figure 4C,D). These data indicate that Rp58 needs to form the Foxg1-Rp58 complex for the efficient binding to the *Robo1, Slit3,* and *Reelin* genes (Figure 5D). Additionally, we found the similar recruitment pattern of Foxg1-Rp58 to the ChIPseq peaks associated with *Neurog2*, *NeuroD1, Rnd2,* and *Unc5D* (Figure S4C,D), which control the differentiation and migration of cortical neurons (Ge et al., 2006; Hand et al., 2005; Heng et al., 2008; Hevner et al., 2006; Miyoshi and Fishell, 2012; Pacary et al., 2011). Together, our results establish that the Foxg1-Rp58 complex binds to the *Robo1, Slit3,* and *Reelin* genes that play essential roles for neuronal migration and projection (Figure 5D).

Foxg1-Rp58 complex represses its target genes in cortical pyramidal neurons

Given that Foxg1 primarily functions as a transcriptional repressor (Kumamoto et al., 2013; Yao et al., 2001), it is possible that the Foxg1-Rp58 complex directly represses the transcription of its target genes in cortical pyramidal neurons, and if so we predicted that the expression of Robo1, Slit3, and Reelin would be derepressed in Foxg1-deficient neurons. To test this possibility, we performed *in situ* hybridization analyses in E16.5 *Foxg1-cKO*,

cHET, and control (Figure 6). In *Foxg1-cKO* brains, the expression pattern of Reelin, Robo1, and Slit3 was drastically altered. The expression domain of Robo1 was markedly expanded to virtually all GFP$^+$ *Foxg1-cKO* cells in the CP, while Robo1 was expressed in the narrower area in control cortices. Likewise, Slit3 is ectopically upregulated in the CP of *Foxg1-cKO* brains, whereas Slit3 expression was hardly detectable in the dorsal cortex of control mice. Ectopic Reelin-expressing cells were dispersed throughout the CP of *Foxg1-cKO* brains, additionally to normal Reelin$^+$ CajalRezius cells in the marginal zone. Our data suggest that the gene repression by the Foxg1-Rp58 complex in post-mitotic cortical neurons is essential to establish the correct expression levels and domains of *Robo1, Slit3,* and *Reelin* in the developing cortex.

The expression domain of other Foxg1-Rp58 target genes was also expanded, and their expression levels were elevated in *Foxg1-cKO* brains (Figure S5A–C). NeuroD1, Rnd2, and Unc5D were aberrantly upregulated in the dorsal and cingulate cortex of *Foxg1-cKO* mice. Ectopic Neurog2$^+$ cells were observed close to the pial surface of *Foxg1-cKO* cortex (*arrowheads*, Figure S5B), suggesting that Neurog2 was derepressed in early-born neurons.

Notably, the expression of all tested Foxg1-Rp58 target genes, including Robo1, Slit3, and Reelin, also increased in *Foxg1-cHET* cortices (Figure 6, S5A–C). The Slit3$^+$ domain was substantially expanded in the cingulate cortex of *Foxg1-cHET*. Remarkably, ectopic Reelin$^+$ and Neurog2$^+$ cells were found in the CP of *Foxg1-cHET* cortices (arrows in Figure 6B, S5B), indicating that the full dosage of *Foxg1* is needed to suppress *Reelin* and *Neurog2* in cortical neurons. To test whether the Foxg1-Rp58 target genes are also dysregulated in global *HET* brains, we monitored the expression levels of the Foxg1-Rp58 target genes in E16.5 *HET* brains. The expression levels of Robo1, Slit3, Neurog2, NeuroD1, Rnd2, and Unc5D significantly increased in global *HET* cortices relative to control littermate *WT* cortices, as shown by the quantitative RTPCR analyses, whereas Rp58 level did not change significantly (Figure S5D), indicating that Foxg1-Rp58 target genes are derepressed in global *HET* cortices. Our analyses indicate that the deletion of a single copy of the *Foxg1* gene in post-mitotic neurons is sufficient to cause dysregulation of expression of Robo1, Slit3, Reelin, and other Foxg1Rp58 target genes, which likely contributes to the cell migratory and axon projection deficits in *Foxg1* het brains.

To monitor a relatively direct outcome of gene regulation by Foxg1-Rp58 *in vivo*, we coexpressed Foxg1 and Rp58 in E14.5 cortex by *in utero* electroporation and examined their target gene expression levels one-day post-electroporation. Misexpression of Foxg1 and Rp58 resulted in a marked repression of the Foxg1-Rp58 target genes *Neurog2*, *Rnd2, NeuroD1* and *Unc5D* in GFP$^+$ transfected cells, compared to the surrounding GFP$^-$ untransfected cells or unelectroporated side of the cortex (Figure S6), indicating that Foxg1-Rp58 functions as a transcriptional repressor in the developing cortex. As the expression of Reelin, Robo1, and Slit3 are very low in the cortex at E14.5, it was not feasible to detect their downregulation using this experimental scheme.

To ask if the upregulation of Robo1 in *Foxg1-cHET* cortex contributes to aberrant callosal pathfinding, we decided to test if lowering Robo levels in *Foxg1-cHET* cells rescue any of callosal misprojection phenotypes. To this end, we removed a copy of *Robo1* and *Robo2*, the

two close paralogs, in *Foxg1-cHET* brains by generating the compound mutant mice *Foxg1*$^{fi/fi}$;*Robo1*$^{+/-}$;*Robo2*$^{fl/+}$;*NEX-Cre*, abbreviated to *Foxg1cHET;Robo1/2 HET*. Intriguingly, *Foxg1-cHET;Robo1/2 HET* mice did not develop the Probst bundle, in contrast to *Foxg1-cHET* mice that show the prominent Probst bundle (Figure 7A), indicating that the lowering Robo levels ameliorates the aberrant accumulation of callosal axons at the midline in *Foxg1-cHET* brains. Despite the evident restoration of callosal axon guidance at the midline, however, the indusium gresium glia still remained underdeveloped in *Foxg1-cHET;Robo1/2 HET* brains (Figure S7). Our results demonstrate that the stalled callosal axons at the midline of *Foxg1-cHET* cortex are, at least partly, attributable to the aberrantly increased Robo levels in *Foxg1-cHET* neurons.

Taken together, our data support the model that in cortical neurons the Foxg1Rp58 complex directly binds and represses a set of genes that control neuronal migration and axonal projection, including Robo1, Slit3, and Reelin, thereby orchestrating the timely integration of cortical neurons into the correct laminar position and subsequent callosal axon navigation (Figure 7B).

DISCUSSION

To decipher the molecular basis of neurodevelopmental and psychiatric disorders, many of which present with interhemispheric connectivity deficits, it is fundamental to decipher the genetic regulation code required for building a functional brain. However, the molecular switches necessary to produce distinct cortical projection neuron subtypes and the genetic programs to establish callosal connections are still far from being fully unraveled. Here we report that Foxg1 plays a key role in pyramidal neurons to orchestrate the development of the cerebral cortex. Further, we show that Robo-Slit signaling is one of the main downstream targets of Foxg1. Complete ablation of *Foxg1* specifically in cortical neurons disrupted cortical layers and caused a loss of upper layer neurons and absence of corpus callosum. Intriguingly, a half gene dosage of *Foxg1* permitted cortical lamination, but it was insufficient for integrating CPNs into the correct layer position and establishing contralateral projection pattern of CPNs, providing a previously unknown molecular mechanism underlying the corpus callosum agenesis in human FOXG1 syndrome.

Foxg1 controls dorso-ventral patterning of the telencephalon and cell proliferation in neural progenitors (Danesin et al., 2009). Then, downregulation of Foxg1 is a prerequisite for neural progenitors to differentiate and migrate through the IZ in the cortex. At a later stage, Foxg1 is upregulated in maturing pyramidal neurons where it promotes the switch from non-radially to radially migrating neurons (Miyoshi and Fishell, 2012). While Foxg1 continues to be expressed in post-migratory pyramidal neurons in the CP, the role of Foxg1 in this context remained unknown. Our study uncovered new roles of Foxg1 in post-migratory pyramidal neurons in establishing cortical layers and axon projections. Together, actions of Foxg1 in both progenitors and pyramidal neurons are required for constructing a functional cerebral cortex. This raises the question of how Foxg1 accomplishes distinct yet essential tasks in different cell types and time points. Our study suggests that the combinatorial action of Foxg1 with other transcription factors serves as a mechanism by which Foxg1 controls cell contextspecific sets of target genes. More specifically, Foxg1 forms a neuron-specific

complex with Rp58 to control proneural and axon guidance genes in cortical pyramidal neurons (Figure 7B). Previous mechanistic and genetic studies are in line with our Foxg1-Rp58 model. Both Foxg1 and Rp58 promote neuronal entry into the CP by triggering the morphological shift from multipolar to bipolar shape (Miyoshi and Fishell, 2012; OhtakaMaruyama et al., 2013). Our genome-wide mapping of Foxg1-binding loci revealed that Foxg1 is recruited to all three known Rp58-target sites controlling *Rnd2*, *Neurog2*, and *NeuroD1* (Heng et al., 2015; Ohtaka-Maruyama et al., 2013; Xiang et al., 2012). Intriguingly, mice and humans with the loss-of-function mutation in the *Rp58/RP58* gene exhibit remarkably similar phenotypes to *Foxg1* mutant mice and FOXG1 syndrome patients. *Rp58*-null mice show microcephaly, defective cortical laminar organization, corpus callosum agenesis and characteristic axon misprojection highly analogous to *Foxg1-cKO* mice (Figure 2C) (Okado et al., 2009; Xiang et al., 2012). In humans, patients possessing *de novo* nonsense mutations in the *RP58* gene or a submicroscopic deletion of the region encoding *RP58* present with intellectual disability, microcephaly and corpus callosum agenesis (de Munnik et al., 2014; Lopes et al., 2016; Perlman et al., 2013; van Bon et al., 2008), like FOXG1 syndrome patients. Notably, *de novo* mutations in *FOXG1* and *RP58* have been found in atypical Rett syndrome patients, suggesting that these patients exhibit overlapping clinical features (Florian et al., 2012; Kortum et al., 2011; Lopes et al., 2016). Together, these findings strongly support our model that the Foxg1-Rp58 complex plays crucial roles in the development of the cerebral cortex in mice and human (Figure 7B). Our model also serves as an excellent example of combinatorial transcription factor code in mammalian brain development. Given that our motif analyses suggest potential partner transcription factors of Foxg1 besides Rp58, Foxg1-directed gene networks are likely to employ cooperation with multiple transcription factors, each of which controls a subset of Foxg1 target genes in a cell context-dependent manner. Additionally, considering that phosphorylation of Foxg1 controls the activity of Foxg1 during normal development and in pathological brain conditions (Baek et al., 2015; Dastidar et al., 2011; Dastidar et al., 2012; Regad et al., 2007), post-translational modification of Foxg1 may function as an additional regulatory layer of Foxg1 activity. As external cues and signal transduction pathways control the phosphorylation of Foxg1, this mechanism could serve as a regulatory point to integrate external signals to Foxg1-directed gene networks.

Our ChIPseq analyses uncovered clusters of Foxg1-Rp58 target genes whose expression is regulated by Foxg1 re-expression in post-mitotic neurons, thus providing key insights into Foxg1-directed gene regulatory networks and human FOXG1 syndrome. We found that Foxg1 is responsible for establishing the correct expression pattern of Robo1 receptor and Slit3 ligand in the CP. Given that Robo1 and Slit3 form an important pathway that controls trajectory and fasciculation of callosal axons in the brain (Andrews et al., 2006; Bagri et al., 2002; Devine and Key, 2008; Lindwall et al., 2007), the callosal misprojection and reduced interhemispheric connectivity in *Foxg1* mutant mice may be attributed, at least in part, to the marked and ectopic induction of Robo1 and Slit3. Supporting this idea, callosal axons of *Foxg1-cHET* neurons did not stall around the midline when Robo levels reduced (Figure 7A). Notably, the developmental deficits of indusium griseum glia in *Foxg1-cHET* brains were not resolved by lowering Robo levels. Given that Slit3 expressed in neurons regulates the midline glia maturation in a non cell-autonomous manner (Unni et al., 2012), the

increased Slit3 levels in *Foxg1-cHET* neurons may contribute to the underdevelopment of the indusium griseum. Our data also suggest that Foxg1 is required for the continuous suppression of Reelin, a key regulator of cortical neuronal migration produced by Cajal-Retzius cells (Franco et al., 2011; Hashimoto-Torii et al., 2008; Jossin and Cooper, 2011), in the CP. Considering that the main cell types of Foxg1 inactvation in *Foxg1-cKO* cortices are neurons, not progenitors (Figure S1), the incresed Reelin likely reflects the transcriptional derepression of the *Reelin* gene in Foxg1-deficient cortical neurons, rather than the cell fate mis-specification of Foxg1-null progenitors. Additionally, Foxg1 was also needed for the timely downregulation of Neurog2, NeuroD1, Rnd2, and Unc5D in cortical projection neurons. While Neurog2, NeuroD1, Rnd2, and Unc5D play important roles in immature neurons, these genes need to be repressed in maturing pyramidal neurons to permit their radial migration (Heng et al., 2015; Miyoshi and Fishell, 2012; Ohtaka-Maruyama et al., 2013; Xiang et al., 2012). Together, the prolonged and deviant expression of cell migratory and axon guidance genes in cortical neurons would be a substantial contributing factor to cortical lamination and axon projection defects and corpus callosum agenesis in *Foxg1* mutant cortices.

Deletions or inactivating mutations in a single allele of *FOXG1* causes FOXG1 syndrome (Florian et al., 2012; Kortum et al., 2011). Duplications of the *FOXG1* gene are also associated with developmental delay, intellectual disability, seizures, and severe speech impairment (Brunetti-Pierri et al., 2011; Yeung et al., 2009). Increased FOXG1 expression levels have been identified as a critical contributing factor to autism spectrum disorder (Mariani et al., 2015). Further, FOXG1 was identified as a highconfidence schizophrenia risk gene by genome-wide association and chromosome conformation studies (Schizophrenia Working Group of the Psychiatric Genomics, 2014; Won et al., 2016). These data highlight that the development and functionality of human brain are highly sensitive to the *FOXG1* dosage. Our study uncovered that, while elimination of Foxg1 in cortical neurons results in profound disruption of all cortical layers, a half of *Foxg1* gene dosage in the same cells allows relatively normal generation of cortical layers but is insufficient to establish correct number and projection pattern of CPNs. These results indicate that diverse actions of Foxg1 are not evenly perturbed by a lower level of Foxg1, and some Foxg1-directed processes are more vulnerable to *Foxg1* gene dosage changes than others. In light of this idea, it is tempting to speculate that the elevated and possibly prolonged expression of FOXG1 in the brains of FOXG1 duplication syndrome patients may lead to not only augmented physiological action of FOXG1, but also gain of the non-physiological FOXG1 action that does not occur in WT brains and is detrimental to brain development. In the future, generation of various animal models, such as *Foxg1* duplication mouse lines, would be useful to understand etiology of FOXG1-involved neurological disorders as well as uncovering the diverse actions of FOXG1 in the healthy brain.

STAR Methods

Key Resources Table

REAGENT or RESOURCE	SOURCE	IDENTIFIER
Antibodies		
mouse anti-GAPDH	Thermo Fisher Scientific	MA1-16757
rabbit anti-Foxg1	Abcam	ab18259
guinea pig anti-Foxg1	Homemade	Epitope used corresponds to amino acids 417–489 of human Foxg1 protein
rabbit anti-Rp58	Proteintech Group	12714-1-AP
mouse anti-FLAG	Sigma	F3165
mouse anti-HA	Biolegend	MMMS-101R
rabbit anti-HA	Bethyl	A190-108A-5
rabbit anti-Pax6	Biolegend	901301
chicken anti-Tbr2	Millipore	AB15894
rabbit anti-Tbr1	Abcam	ab31940
rat anti-Ctip2	Abcam	ab18465
mouse anti-Satb2	Abcam	ab51502
rabbit anti-Cux1	SantaCruz	sc-13024
rat anti-L1	Millipore	MAB5272
rabbit anti-GFAP	Dako	Z0334
rabbit anti-GFP	Thermo Fisher Scientific	A11122
anti-digoxigenin-alkaline phosphatase (AP)	Roche	11093274910
DNA Plasmids		
Mouse Foxg1 cDNA	Dr. Stifani	Montreal Neurological Institute and Hospital
FLAG-Foxg1-pcDNA3		
FLAG-Foxg1pCIG2.2iresGFP		
Mouse RP58 cDNA	Drs. Ohtaka-Maruyama and Okado	Tokio Metropolitan Institute of Medical Science
HA-Rp58-pcDNA3		
HA-Rp58-CIG2.2iresGFP		
pCAG-CRE-T2A-tdTomato		
pCAG-T2A-tdTomato		
mNeuroD1-pCS2	Dr. Lee, JE	University of Colorado
mRnd2-pT7T3DPac	Dr. Guillemot	The Francis Crick Institute
mSlit3	Dr. Ornitz	Washington University
mUnc5D-pBluescriptSK(−)		
mReelin-pBluescriptSK(−)		
CTGF-pBluescriptSK(−)		
FLP-pBluescriptSK(−)		
qRT-PCR DNA Primers		
mouse Foxg1	Integrated DNA Technologies	forward (5’- AGGCTGACGCACTTGGAG -3’)
		reverse (5’-GCTTCTCGTACTTGCCGTTC-3’)
mouse Rp58		forward (5’-TGCCCAGTGATGAAGATGAA-3’)
		reverse (5’- CTCCTGAAAGGCTGGACTTG-3’)
mouse Rnd2		forward (5’-AGTGGGAGCTGTGTCCTACG-3’)
		reverse (5’- GTCCCGACAGTTGAGTGGAT-3’)
mouse Neurog2		forward (5’-ACCTCCACGTCCCCATACAG -3’)
		reverse (5’-AGGTGAGGCGCATAACGATG-3’)
mouse NeuroD1		forward (5’-CTTGAAGCCATGAATGCAGAGG -3’)
		reverse (5’-AGAGCGTCTGTACGAAGGAGAC-3’)
mouse Reelin		reverse (5’-GAACACCAGTGATAGTCCTGATTCT-3’)
mouse Unc5D		forward (5’-CACCAGGGCTGACCATAACT-3’)

REAGENT or RESOURCE	SOURCE	IDENTIFIER
		reverse (5'-TCTACCACAGCGAACATTGC-3')
mouse Robo1		forward (5'-TAATGAGTTTCAAGGAGCAGACAG-3')
		reverse (5'-CGAGACACCAAACCTTATATTCTTG-3')
mouse Slit3		forward (5'-TGGTACTCTATGGGAACAAGATCAC-3')
		reverse (5'-GAGAGAGCAGATTGAGGTTCTGTAG-3')
ChIP DNA Primers		
mouse Unc5D, peak 22353	Integrated DNA Technologies	forward (5'-TGGCAAATACTCACAACACC-3')
		reverse (5'-TGATTGTCTCATTGTCTTAAACTGAA-3')
mouse Neurog2, peak 15392		forward (5'-ATCTTCAGAGTGGCAGAACAGAT-3')
		reverse (5'-TGGGAGTTTCTAGTGCTTATTTCAC-3')
mouse Rnd2, peak 4092		forward (5'-GTAGCCAGAGACGAGAGAGATGTA-3')
		reverse (5'-GGGTTCATCCTGACACTGAAT-3')
mouse NeuroD1, peak 13192		forward (5'-AAGCTATTGGATGGAGGATGG -3')
		reverse (5'-GAGGCGGAGGTGTATTCTCTC-3')
mouse Robo1, peak 9560		forward (5'-AGGTTGGCTTGCTTTCTATCAG-3')
		reverse (5'-AACATGGGAGTGGCTTACTTTATC-3')
mouse Slit3, peak 3196		forward (5'-CCTCCTCATCAAAGACCCAAAT-3')
		reverse (5'-TAGCAGCCAAAGCAATAAcagc-3')
mouse Reelin, peak 17512		forward (5'-GTCTGGTGAAGACAACTGAATCC-3')
		reverse (5'-GAGCTACAACTCCTGCATGTAAA-3')
Experimental Models: Organisms/Strains, Cell lines		
HEK293	ATCC	CRL_1573
Foxg1tm1(cre)Skm	Jackson Laboratory	(Hebert and McConnell, 2000)
Foxg1 fi/fi		(Miyoshi and Fishell, 2012)
NEX-Cre		(Goebbels et al., 2006)
Robo1$^{+/-}$		(Long et al., 2004)
Robo2 fi/fi		(Lu et al., 2007)
Software		
ApE	http://jorgensen.biology.utah.edu/wayned/ape/	V2.0.47
Fiji	https://imagej.net/Fiji	
GraphPad Prism	https://www.graphpad.com/scientific-software/prism/	Version 5.0f
Zen	Zeiss	
ImageScope	https://www.leicabiosystems.com/digital-pathology/manage/aperio-imagescope/	
MACS tool for peak calling		(Zhang et al., 2008)
MEME Suite tools	http://meme-suite.org	(Bailey et al., 2009)

Contact for Reagent and Resource Sharing

Further information and requests for resources and reagents should be directed to and will be fulfilled by the Lead Contact, Dr. Soo-Kyung Lee (leesoo@ohsu.edu)

Experimental Model and Subject Details

All animal procedures were conducted in accordance with the Guidelines for the Care and Use of Laboratory Animals and were approved by the Institutional Animal Care and Use Committee (IACUC) at OHSU. Animals aged from embryonic day E16.5 to postnatal day P30 were used as indicated in each figure and figure legend. No significant differences based on sex were observed, and data were pooled between sexes.

Method Details

Cell cultures and transfections.—HEK293 cells were grown in Dulbecco's Modified Eagle's Medium (DMEM) supplemented with 10% fetal bovine serum (HyClone), 1% Penicillin/Streptomycin solution (HyClone) and 1% L-Glutamine 200mM (Gibco). Transfection of HEK293 cells was performed using 60% confluent cultures using Lipofectamine 2000 transfecting reagent (Thermo Fisher Scientific) according to manufactory instructions. In all transfections, the amounts of plasmid DNA were adjusted on a molar basis, and the total quantity of DNA in the transfection mixture was kept constant by the addition of pBluescriptSK(−) (Stratagene, Inc.) for immunoprecipitation experiments.

DNA constructs.—For *FLAG-Foxg1-pcDNA3* plasmid, mouse Foxg1 cDNA was cloned in pcDNA3 vector between 5'EcoRI and 3' XhoI. Three copies (3X) of FLAG tag were cloned upstream and in frame with Foxg1 between 5'HindIII and 3'EcoRI. For *FLAGFoxg1-pCIG2.2iresGFP* plasmid, mouse Foxg1 cDNA was cloned in pCIG2.2iresGFP vector between 5'EcoRI and 3'PstI. 3XFLAG tag was cloned upstream and in frame with Foxg1 between 5'XhoI and 3'EcoRI. For *HA-Rp58-pcDNA3* plasmid, mouse Rp58 cDNA was cloned in pcDNA3 between 5'EcoRV and 3'XhoI. Three copies (3X) of HA tag were cloned upstream and in frame with Rp58 between 5'BamHI and 3'EcoRV. For *HA-Rp58-CIG2.2iresGFP* plasmid, 3XHA-mRp58 DNA fragment was amplified by PCR to add XhoI site at the 5' and SmaI site at 3' ends of the DNA fragment. 3XHA-mRp58 was then cloned in pCIG2.2iresGFP between 5'XhoI and 3'SmaI. *pCAG-CRE-T2AtdTomato* was generated by cloning CRE coding sequence in frame with T2A peptide in *pCAG-T2A-tdTomato*. For *mUnc5D-pBluescriptSK(−),* mouse Unc5D cDNA fragment (1800 bp) was amplified from total RNA of E15.5 brains and cloned in pBluescriptSK(−) between 5' HindIII and 3'EcoRI. For *mReelin-pBluescriptSK(−),* mouse Reelin cDNA fragment (1–993 bp) was amplified from total RNA of E15.5 brains and cloned in pBluescriptSK(−) between 5' HindIII and 3'EcoRI. For *Neuropilin-1-pBluescript,* mouse Neuropilin-1 cDNA fragment (1–917 bp) was amplified from total RNA of E15.5 brains and cloned in pBluescriptSK(−) between 5' HindIII and 3'EcoRI. For *CTGFpBluescriptSK(−),* mouse CTGF cDNA fragment (17–517 bp) was amplified from total RNA of E15.5 brains and cloned in pBluescriptSK(−) between 5' HindIII and 3'EcoRI. For *FLP-pBluescriptSK(−),* recombinase flippase DNA fragment (308–1108 bp) was amplified from *Foxg1* $^{fi/fi}$ mice genomic DNA and cloned in pBluescriptSK(−) between 5' HindIII and 3'EcoRI.

Western blotting analyses.—Thirty micrograms of total brain extracts of indicated ages or HEK293 cells were separated on 8% SDS-PAGE gel and transferred to nitrocellulose membranes (Schleicher & Schuell). The membranes were blocked in 10% nonfat dry milk, 20 mM Tris-HCl, pH 7.5, 150 mM NaCl, 0.1% Tween20, followed by incubation with primary antibodies for 2 hours at room temperature. Then, secondary antibodies conjugated with horseradish peroxidase were added and incubated for 1 hour. Proteins were detected using chemiluminescent Super Signal West Dura kit (Thermo Scientific).

Co-immunoprecipitation analyses.—Cortices of indicated stage or transfected HEK293 cells were homogenized and incubated for 2 hours on rotation at 4ºC in RIPA buffer (50mM Tris-HCl pH8, 0.5mM EDTA pH8, 1% Triton X-100, 0.5% Sodium

deoxycholate, 150mM NaCl, 10% glycerol, protease and phosphatase inhibitors). The lysate was spun down and subject to immunoprecipitation using 1 μg of the indicated antibody or rabbit/mouse IgG with constant rotation overnight at 4ºC, followed by 3 hours with Protein A/G agarose beads (Thermo Fisher Scientific). Immunoprecipitates were washed three times on ice using RIPA buffer with constant rotation. Next, beads were re-suspended in SDS loading buffer and analyzed by Western blotting analyses.

RNA Isolation, RT-PCR, and quantitative real-time RT-PCR analyses.—Total RNA from indicated stages was prepared using Trizol (Thermo Fisher Scientific) and treated with RNase-free DNase (Thermo Fisher Scientific). For reverse transcription, First Strand Superscript III (Invitrogen) was used and quantitative real-time PCR was performed in a LightCycler 96 System (Roche) using FastStart Essential DNA Green Master (Roche) under the same cycling conditions. Relative abundance of each cDNA was determined according to the standard curve and normalized to 18S RNA levels. Measurements represent gene specific mRNA fold enrichment over the mRNA of housekeeping gene GAPDH (n=3 brains/genotype, run in duplicates).

ChIP analyses.—Chromatin immunoprecipitation was carried as described previously(Lee et al., 2013) with some modifications. Briefly, two embryonic cortices/genotype were mechanically homogenized, and cross-linked chromatin was sonicated to generate fragments with an average length of 300–400 bp. The chromatin was subjected to immunoprecipitation using 1 μg of anti-Foxg1 and anti-Rp58 antibodies or rabbit IgG. After reversal of cross-links, DNA and 10% input samples were purified using standard phenol:chloroform purification followed by ethanol precipitation. For qRT-PCR analyses, primers were designed within 300–500 bp of the Foxg1 or Rp58 DNA binding site, and ChIP DNA amounts were determined from standard curve and normalized to the input DNA. All experiments were run in duplicate and repeated three independent times.

ChIPseq analyses.—ChIP was performed using Foxg1 antibodies (Santa Cruz) in E14.5E15.5 wild-type embryos. Then the ChIP DNA samples from two biologically independent ChIP experiments as well as input DNA sample were sequenced on the Illumina Hiseq2000 platform (pair-end, 50mer). The sequencing reads were mapped to the mouse reference genome (mm9 on UCSC genome browser) after exclusion of multiple-hit or low-mapping-quality reads. MACS tool for peak calling (Zhang et al., 2008) was applied to identify Foxg1-bound ChIPseq peaks using the default setting. The binding sites were annotated to genes with the following criterion: at least one ChIPseq peak located from 2kb upstream or downstream of a gene. If no gene was found within the selected range from a peak, the nearest genes to the peak were chosen as potential targets. MEME Suite tools (Bailey et al., 2009) (http://memesuite.org) were used to discover motifs in +/−200 bp sequences from the summit of top 2000 peaks ranked by the fold enrichment. The resulting motifs were compared with databases of known motifs (e.g., JASPAR) using TOMTOM (Gupta et al., 2007) that is also included in MEME suite (Bailey et al., 2009). DAVID (Huang da et al., 2009) (Database for Annotation, Visualization and Integration Discovery, https://david.ncifcrf.gov) based on Gene Ontology (GO) terms was performed for functional

enrichment analysis. Assessments were considered significant with $p < 0.05$. ChIPseq data was deposited in the Gene Expression Omnibus (GEO) database (accession #: GSE96070).

***In utero* electroporation.—**For *in utero* electroporation, timed-pregnant Foxg1 $^{fi/fi}$ females crossed with Foxg1$^{fi/+}$*NEX-Cre* males, Foxg1 $^{fi/fi}$ females crossed with C57BL/6N males, C57BL/6N females crossed with global *HET* males were anesthetized at E15.5 with isoflurane (4% during induction, 2.5% during surgery), and the uterine horns were exposed by way of laparotomy. 1 μg of the expression vector in PBS containing 0.05% fast green (Sigma-Aldrich, St Louis, MO, USA) was injected into the lateral ventricle of the embryo using a 100 μm glass capillary (1B100–4, World Precision Instruments, Inc., USA). Electroporation was performed using Tweezertrodes (diameter, 5 mm; BTX, Holliston, MA, USA) with 5 pulses (30V for E13.5 embryos and 35V for E15.5 embryos) for 50 millisecond duration and 950 millisecond intervals using a square-wave pulse generator (ECM 830; BTX). The uterine horns were then returned to the abdominal cavity, the wall and skin were sutured, and embryos were allowed to continue their normal development and collected for the further analyses at indicated stages.

DiI injections.—Small crystals of DiI (Thermo Fisher Scientific) were applied on the surface of the cerebral somatosensory area. Brains were stored in the dark at 37°C for at least 4 weeks to allow DiI transport and then vibratome-sectioned at 150 μm.

Immunohistochemistry and quantifications.—Embryonic heads (E16.5) and dissected brains (P0-P7) were fixed in 4% formalin in phosphate-buffered saline (PBS) at 4°C overnight, equilibrated in 30% sucrose and embedded in TFM tissue frozen medium (Electron Microscopy Sciences) for frozen sectioning. Age and position matched sections were dried, post-fixed with cold acetone and stained using standard immunohistochemical techniques. Sections were stained with secondary speciesspecific antibodies conjugated to Alexa-488, Alexa-555, or Alexa-647 (Jackson ImmunoResearch), and counterstained with DAPI to reveal nuclei. Images from 14 μmthick immunostained brain sections were acquired through optical sectioning with an ApoTome.2 on an AxioImager.Z1 epifluorescence microscope using Zen Software and AxioCam 506 (Zeiss). Images were further processed using Fiji (Schindelin et al., 2012) and Photoshop CS4 (Adobe, San Jose, CA). Quantifications of neuronal migration after *in utero* electroporation experiments were performed using age-specified bins (indicated in figure legends) in sections spanning at least 100μm of cortex. Foxg1 expression quantification (Figure S1B) was determined by calculating CTCF (Corrected Total Cell Fluorescence), which is [ROI Integrated Density - (Fluorescence measured Area*mean fluorescence background readings)]. In brief, one Region of Interest (ROI) (x=200μm; y=600μm) per each brain slice immunostained with Foxg1 antibody was converted to 8 bits. Integrated Density per each slice was obtained averaging the measurements from 4 (50μmx50μm) areas/slice expressing Foxg1. Mean Fluorescence Background was obtained averaging the measurements from 4 (50μmx50μm) areas/slice not expressing Foxg1. Each point of the quantification graph represents one brain slice.

In situ* hybridization analyses.—In situ* hybridization analyses were carried out on 18 μm thick frozen brain sections according to standard procedures. Digoxigenin-labeled antisense RNA probes were hybridized to brain sections at 68°C. Hybridized sections were washed, incubated with anti-digoxigenin-alkaline phosphatase (AP) antibody, and then subjected to color reaction. For in situ hybridization-immunofluorescence double experiments, consecutive brain slices of E14.5 *in utero* electroporated brains harvested at E15.5 were analyzed. n=3 brains/probe/DNA. Images were acquired by an Aperio Digital Whole Slide Scanner (Leica Biosystems) to assure uniformity of background throughout different experiments.

Cresyl violet staining.—Cresyl Violet staining was carried out on 25 μm thick frozen brain sections according to standard procedures. Images were acquired by an Aperio Digital Whole Slide Scanner (Leica Biosystems) to assure uniformity of background throughout different experiments.

Statistics.—The data were analyzed with independent two-tailed samples t-tests or oneway ANOVA followed up by *post hoc* tests. Normality was checked with the ShapiroWilk criterion and, when violated, non-parametric statistics were applied (MannWhitney). Data normally distributed were analyzed by unpaired two-tailed t-test for twogroup comparisons. When Levene's test for the equality of variances was significant, suggesting that equal variances could be not assumed, Welch's correction was used and the adjusted values and degrees of freedom are reported. One-way ANOVA followed, when appropriate (p<0.05), by Tukey *post hoc* test was used for comparisons of more than two groups. All bars and error bars represent the mean ± S.D., and significance was set at $p < 0.05$ (****, p <0.0001;*** $p <$ 0.001;** $p < 0.01$;* $p < 0.05$; *ns*, not significant). The data were analyzed using GraphPad Prism 5 (GraphPad, La Jolla, CA), and the graphs were created using GraphPad Prism 5.

Supplementary Material

Refer to Web version on PubMed Central for supplementary material.

ACKNOWLEDGEMENTS

We are grateful to Younjung Park for managing mouse colonies, generating antibodies, and excellent technical helps, Gord Fishell and Goichi Miyoshi for *Foxg1*-floxed mice, Klaus-Armin Nave for *NEX-Cre* mice, Richard Maas for *Robo* mice, Paul Barnes and Kevin Wright for critical discussion and comments on the manuscript, and the Lee lab members for helpful discussion. This research was supported by grants from NIH/NINDS (R01NS054941, R56NS054941, and R01NS100471 to S.-K.L., R01NS089777 to B.C., P30NS061800 to Advanced Light Microscopy Core, OHSU), NIH/NIDDK (R01DK064678 to J.W.L., R01DK103661 to J.W.L. and S.-K.L.), NIH/NIMH (R01MH094589 to B.C.), American Heart Association (to S.-K.L.), and Blackswan foundation and FOXG1 research foundation (to J.W.L. and S.-K.L.).

REFERENCES

Andrews W, Liapi A, Plachez C, Camurri L, Zhang J, Mori S, Murakami F, Parnavelas JG, Sundaresan V, and Richards LJ (2006). Robo1 regulates the development of major axon tracts and interneuron migration in the forebrain. Development 133, 2243–2252. [PubMed: 16690755]

Baek ST, Copeland B, Yun EJ, Kwon SK, Guemez-Gamboa A, Schaffer AE, Kim S, Kang HC, Song S, Mathern GW, et al. (2015). An AKT3-FOXG1-reelin network underlies defective migration in human focal malformations of cortical development. Nat Med 21, 1445–1454. [PubMed: 26523971]

Bagri A, Marin O, Plump AS, Mak J, Pleasure SJ, Rubenstein JL, and Tessier-Lavigne M (2002). Slit proteins prevent midline crossing and determine the dorsoventral position of major axonal pathways in the mammalian forebrain. Neuron 33, 233–248. [PubMed: 11804571]

Bailey TL, Boden M, Buske FA, Frith M, Grant CE, Clementi L, Ren J, Li WW, and Noble WS (2009). MEME SUITE: tools for motif discovery and searching. Nucleic Acids Res 37, W202–208. [PubMed: 19458158]

Brunetti-Pierri N, Paciorkowski AR, Ciccone R, Della Mina E, Bonaglia MC, Borgatti R, Schaaf CP, Sutton VR, Xia Z, Jelluma N, et al. (2011). Duplications of FOXG1 in 14q12 are associated with developmental epilepsy, mental retardation, and severe speech impairment. Eur J Hum Genet 19, 102–107. [PubMed: 20736978]

Danesin C, Peres JN, Johansson M, Snowden V, Cording A, Papalopulu N, and Houart C (2009). Integration of telencephalic Wnt and hedgehog signaling center activities by Foxg1. Dev Cell 16, 576–587. [PubMed: 19386266]

Dastidar SG, Landrieu PM, and D'Mello SR (2011). FoxG1 promotes the survival of postmitotic neurons. J Neurosci 31, 402–413. [PubMed: 21228151]

Dastidar SG, Narayanan S, Stifani S, and D'Mello SR (2012). Transducin-like enhancer of Split-1 (TLE1) combines with Forkhead box protein G1 (FoxG1) to promote neuronal survival. J Biol Chem 287, 14749–14759. [PubMed: 22354967]

de Munnik SA, Garcia-Minaur S, Hoischen A, van Bon BW, Boycott KM, Schoots J, Hoefsloot LH, Knoers NV, Bongers EM, and Brunner HG (2014). A de novo non-sense mutation in ZBTB18 in a patient with features of the 1q43q44 microdeletion syndrome. Eur J Hum Genet 22, 844–846. [PubMed: 24193349]

Devine CA, and Key B (2008). Robo-Slit interactions regulate longitudinal axon pathfinding in the embryonic vertebrate brain. Dev Biol 313, 371–383. [PubMed: 18061159]

Eagleson KL, Schlueter McFadyen-Ketchum LJ, Ahrens ET, Mills PH, Does MD, Nickols J, and Levitt P (2007). Disruption of Foxg1 expression by knock-in of cre recombinase: effects on the development of the mouse telencephalon. Neuroscience 148, 385–399. [PubMed: 17640820]

Florian C, Bahi-Buisson N, and Bienvenu T (2012). FOXG1-Related Disorders: From Clinical Description to Molecular Genetics. Mol Syndromol 2, 153–163. [PubMed: 22670136]

Franco SJ, Martinez-Garay I, Gil-Sanz C, Harkins-Perry SR, and Muller U (2011). Reelin regulates cadherin function via Dab1/Rap1 to control neuronal migration and lamination in the neocortex. Neuron 69, 482–497. [PubMed: 21315259]

Ge W, He F, Kim KJ, Blanchi B, Coskun V, Nguyen L, Wu X, Zhao J, Heng JI, Martinowich K, et al. (2006). Coupling of cell migration with neurogenesis by proneural bHLH factors. Proc Natl Acad Sci U S A 103, 1319–1324. [PubMed: 16432194]

Goebbels S, Bormuth I, Bode U, Hermanson O, Schwab MH, and Nave KA (2006). Genetic targeting of principal neurons in neocortex and hippocampus of NEX-Cre mice. Genesis 44, 611–621. [PubMed: 17146780]

Greig LC, Woodworth MB, Galazo MJ, Padmanabhan H, and Macklis JD (2013). Molecular logic of neocortical projection neuron specification, development and diversity. Nat Rev Neurosci 14, 755–769. [PubMed: 24105342]

Gupta S, Stamatoyannopoulos JA, Bailey TL, and Noble WS (2007). Quantifying similarity between motifs. Genome Biol 8, R24. [PubMed: 17324271]

Hanashima C, Shen L, Li SC, and Lai E (2002). Brain factor-1 controls the proliferation and differentiation of neocortical progenitor cells through independent mechanisms. J Neurosci 22, 6526–6536. [PubMed: 12151532]

Hand R, Bortone D, Mattar P, Nguyen L, Heng JI, Guerrier S, Boutt E, Peters E, Barnes AP, Parras C, et al. (2005). Phosphorylation of Neurogenin2 specifies the migration properties and the dendritic morphology of pyramidal neurons in the neocortex. Neuron 48, 45–62. [PubMed: 16202708]

Hardcastle Z, and Papalopulu N (2000). Distinct effects of XBF-1 in regulating the cell cycle inhibitor p27(XIC1) and imparting a neural fate. Development 127, 1303–1314. [PubMed: 10683182]

Hashimoto-Torii K, Torii M, Sarkisian MR, Bartley CM, Shen J, Radtke F, Gridley T, Sestan N, and Rakic P (2008). Interaction between Reelin and Notch signaling regulates neuronal migration in the cerebral cortex. Neuron 60, 273–284. [PubMed: 18957219]

Hebert JM, and McConnell SK (2000). Targeting of cre to the Foxg1 (BF-1) locus mediates loxP recombination in the telencephalon and other developing head structures. Dev Biol 222, 296–306. [PubMed: 10837119]

Heng JI, Nguyen L, Castro DS, Zimmer C, Wildner H, Armant O, SkowronskaKrawczyk D, Bedogni F, Matter JM, Hevner R, et al. (2008). Neurogenin 2 controls cortical neuron migration through regulation of Rnd2. Nature 455, 114–118. [PubMed: 18690213]

Heng JI, Qu Z, Ohtaka-Maruyama C, Okado H, Kasai M, Castro D, Guillemot F, and Tan SS (2015). The zinc finger transcription factor RP58 negatively regulates Rnd2 for the control of neuronal migration during cerebral cortical development. Cereb Cortex 25, 806816.

Hevner RF, Hodge RD, Daza RA, and Englund C (2006). Transcription factors in glutamatergic neurogenesis: conserved programs in neocortex, cerebellum, and adult hippocampus. Neurosci Res 55, 223–233. [PubMed: 16621079]

Huang da W, Sherman BT, and Lempicki RA (2009). Systematic and integrative analysis of large gene lists using DAVID bioinformatics resources. Nat Protoc 4, 44–57. [PubMed: 19131956]

Jossin Y, and Cooper JA (2011). Reelin, Rap1 and N-cadherin orient the migration of multipolar neurons in the developing neocortex. Nat Neurosci 14, 697–703. [PubMed: 21516100]

Kortum F, Das S, Flindt M, Morris-Rosendahl DJ, Stefanova I, Goldstein A, Horn D, Klopocki E, Kluger G, Martin P, et al. (2011). The core FOXG1 syndrome phenotype consists of postnatal microcephaly, severe mental retardation, absent language, dyskinesia, and corpus callosum hypogenesis. J Med Genet 48, 396–406. [PubMed: 21441262]

Kumamoto T, Toma K, Gunadi, McKenna WL, Kasukawa T, Katzman S, Chen B, and Hanashima C (2013). Foxg1 coordinates the switch from nonradially to radially migrating glutamatergic subtypes in the neocortex through spatiotemporal repression. Cell Rep 3, 931–945. [PubMed: 23523356]

Lee S, Shen R, Cho HH, Kwon RJ, Seo SY, Lee JW, and Lee SK (2013). STAT3 promotes motor neuron differentiation by collaborating with motor neuron-specific LIM complex. Proc Natl Acad Sci U S A 110, 11445–11450. [PubMed: 23798382]

Lindwall C, Fothergill T, and Richards LJ (2007). Commissure formation in the mammalian forebrain. Curr Opin Neurobiol 17, 3–14. [PubMed: 17275286]

Long H, Sabatier C, Ma L, Plump A, Yuan W, Ornitz DM, Tamada A, Murakami F, Goodman CS, and Tessier-Lavigne M (2004). Conserved roles for Slit and Robo proteins in midline commissural axon guidance. Neuron 42, 213–223. [PubMed: 15091338]

Lopes F, Barbosa M, Ameur A, Soares G, de Sa J, Dias AI, Oliveira G, Cabral P, Temudo T, Calado E, et al. (2016). Identification of novel genetic causes of Rett syndrome-like phenotypes. J Med Genet 53, 190–199. [PubMed: 26740508]

Lu W, van Eerde AM, Fan X, Quintero-Rivera F, Kulkarni S, Ferguson H, Kim HG, Fan Y, Xi Q, Li QG, et al. (2007). Disruption of ROBO2 is associated with urinary tract anomalies and confers risk of vesicoureteral reflux. Am J Hum Genet 80, 616–632. [PubMed: 17357069]

Mariani J, Coppola G, Zhang P, Abyzov A, Provini L, Tomasini L, Amenduni M, Szekely A, Palejev D, Wilson M, et al. (2015). FOXG1-Dependent Dysregulation of GABA/Glutamate Neuron Differentiation in Autism Spectrum Disorders. Cell 162, 375–390. [PubMed: 26186191]

Martynoga B, Morrison H, Price DJ, and Mason JO (2005). Foxg1 is required for specification of ventral telencephalon and region-specific regulation of dorsal telencephalic precursor proliferation and apoptosis. Dev Biol 283, 113–127. [PubMed: 15893304]

Miyoshi G, and Fishell G (2012). Dynamic FoxG1 expression coordinates the integration of multipolar pyramidal neuron precursors into the cortical plate. Neuron 74, 1045–1058. [PubMed: 22726835]

Ohtaka-Maruyama C, Hirai S, Miwa A, Heng JI, Shitara H, Ishii R, Taya C, Kawano H, Kasai M, Nakajima K, et al. (2013). RP58 regulates the multipolar-bipolar transition of newborn neurons in the developing cerebral cortex. Cell Rep 3, 458–471. [PubMed: 23395638]

Okado H, Ohtaka-Maruyama C, Sugitani Y, Fukuda Y, Ishida R, Hirai S, Miwa A, Takahashi A, Aoki K, Mochida K, et al. (2009). The transcriptional repressor RP58 is crucial for cell-division patterning and neuronal survival in the developing cortex. Dev Biol 331, 140–151. [PubMed: 19409883]

Pacary E, Heng J, Azzarelli R, Riou P, Castro D, Lebel-Potter M, Parras C, Bell DM, Ridley AJ, Parsons M, et al. (2011). Proneural transcription factors regulate different steps of cortical neuron migration through Rnd-mediated inhibition of RhoA signaling. Neuron 69, 1069–1084. [PubMed: 21435554]

Paul LK, Brown WS, Adolphs R, Tyszka JM, Richards LJ, Mukherjee P, and Sherr EH (2007). Agenesis of the corpus callosum: genetic, developmental and functional aspects of connectivity. Nat Rev Neurosci 8, 287–299. [PubMed: 17375041]

Perlman SJ, Kulkarni S, Manwaring L, and Shinawi M (2013). Haploinsufficiency of ZNF238 is associated with corpus callosum abnormalities in 1q44 deletions. Am J Med Genet A 161A, 711–716. [PubMed: 23494996]

Regad T, Roth M, Bredenkamp N, Illing N, and Papalopulu N (2007). The neural progenitor-specifying activity of FoxG1 is antagonistically regulated by CKI and FGF. Nat Cell Biol 9, 531–540. [PubMed: 17435750]

Schindelin J, Arganda-Carreras I, Frise E, Kaynig V, Longair M, Pietzsch T, Preibisch S, Rueden C, Saalfeld S, Schmid B, et al. (2012). Fiji: an open-source platform for biologicalimage analysis. Nat Methods 9, 676–682. [PubMed: 22743772]

Schizophrenia Working Group of the Psychiatric Genomics, C. (2014). Biological insights from 108 schizophrenia-associated genetic loci. Nature 511, 421–427. [PubMed: 25056061]

Seoane J, Le HV, Shen L, Anderson SA, and Massague J (2004). Integration of Smad and forkhead pathways in the control of neuroepithelial and glioblastoma cell proliferation. Cell 117, 211–223. [PubMed: 15084259]

Shen L, Nam HS, Song P, Moore H, and Anderson SA (2006). FoxG1 haploinsufficiency results in impaired neurogenesis in the postnatal hippocampus and contextual memory deficits. Hippocampus 16, 875–890. [PubMed: 16941454]

Siegenthaler JA, and Miller MW (2008). Generation of Cajal-Retzius neurons in mouse forebrain is regulated by transforming growth factor beta-Fox signaling pathways. Dev Biol 313, 35–46. [PubMed: 18005957]

Siegenthaler JA, Tremper-Wells BA, and Miller MW (2008). Foxg1 haploinsufficiency reduces the population of cortical intermediate progenitor cells: effect of increased p21 expression. Cereb Cortex 18, 1865–1875. [PubMed: 18065723]

Smith KM, Ohkubo Y, Maragnoli ME, Rasin MR, Schwartz ML, Sestan N, and Vaccarino FM (2006). Midline radial glia translocation and corpus callosum formation require FGF signaling. Nat Neurosci 9, 787–797. [PubMed: 16715082]

Tao W, and Lai E (1992). Telencephalon-restricted expression of BF-1, a new member of the HNF-3/fork head gene family, in the developing rat brain. Neuron 8, 957–966. [PubMed: 1350202]

Unni DK, Piper M, Moldrich RX, Gobius I, Liu S, Fothergill T, Donahoo AL, Baisden JM, Cooper HM, and Richards LJ (2012). Multiple Slits regulate the development of midline glial populations and the corpus callosum. Dev Biol 365, 36–49. [PubMed: 22349628]

van Bon BW, Koolen DA, Borgatti R, Magee A, Garcia-Minaur S, Rooms L, Reardon W, Zollino M, Bonaglia MC, De Gregori M, et al. (2008). Clinical and molecular characteristics of 1qter microdeletion syndrome: delineating a critical region for corpus callosum agenesis/hypogenesis. J Med Genet 45, 346–354. [PubMed: 18178631]

Won H, de la Torre-Ubieta L, Stein JL, Parikshak NN, Huang J, Opland CK, Gandal MJ, Sutton GJ, Hormozdiari F, Lu D, et al. (2016). Chromosome conformation elucidates regulatory relationships in developing human brain. Nature 538, 523–527. [PubMed: 27760116]

Wu SX, Goebbels S, Nakamura K, Nakamura K, Kometani K, Minato N, Kaneko T, Nave KA, and Tamamaki N (2005). Pyramidal neurons of upper cortical layers generated by NEX-positive progenitor cells in the subventricular zone. Proc Natl Acad Sci U S A 102, 17172–17177. [PubMed: 16284248]

Xiang C, Baubet V, Pal S, Holderbaum L, Tatard V, Jiang P, Davuluri RV, and Dahmane N (2012). RP58/ZNF238 directly modulates proneurogenic gene levels and is required for neuronal differentiation and brain expansion. Cell Death Differ 19, 692–702. [PubMed: 22095278]

Xuan S, Baptista CA, Balas G, Tao W, Soares VC, and Lai E (1995). Winged helix transcription factor BF-1 is essential for the development of the cerebral hemispheres. Neuron 14, 1141–1152. [PubMed: 7605629]

Yao J, Lai E, and Stifani S (2001). The winged-helix protein brain factor 1 interacts with groucho and hes proteins to repress transcription. Mol Cell Biol 21, 1962–1972. [PubMed: 11238932]

Yeung A, Bruno D, Scheffer IE, Carranza D, Burgess T, Slater HR, and Amor DJ (2009). 4.45 Mb microduplication in chromosome band 14q12 including FOXG1 in a girl with refractory epilepsy and intellectual impairment. Eur J Med Genet 52, 440–442. [PubMed: 19772934]

Zhang Y, Liu T, Meyer CA, Eeckhoute J, Johnson DS, Bernstein BE, Nusbaum C, Myers RM, Brown M, Li W, et al. (2008). Model-based analysis of ChIP-Seq (MACS). Genome Biol 9, R137. [PubMed: 18798982]

HIGHLIGHTS

- Foxg1 deficiency in cortical neurons led to corpus callosum agenesis
- Loss of only one *Foxg1* copy in neurons made callosal axons stalled at the midline
- Foxg1 cooperates with Rp58 to repress key axon guidance genes in cortical neurons
- Lowering Robo levels in *Foxg1* heterozygous brains restored callosal projection

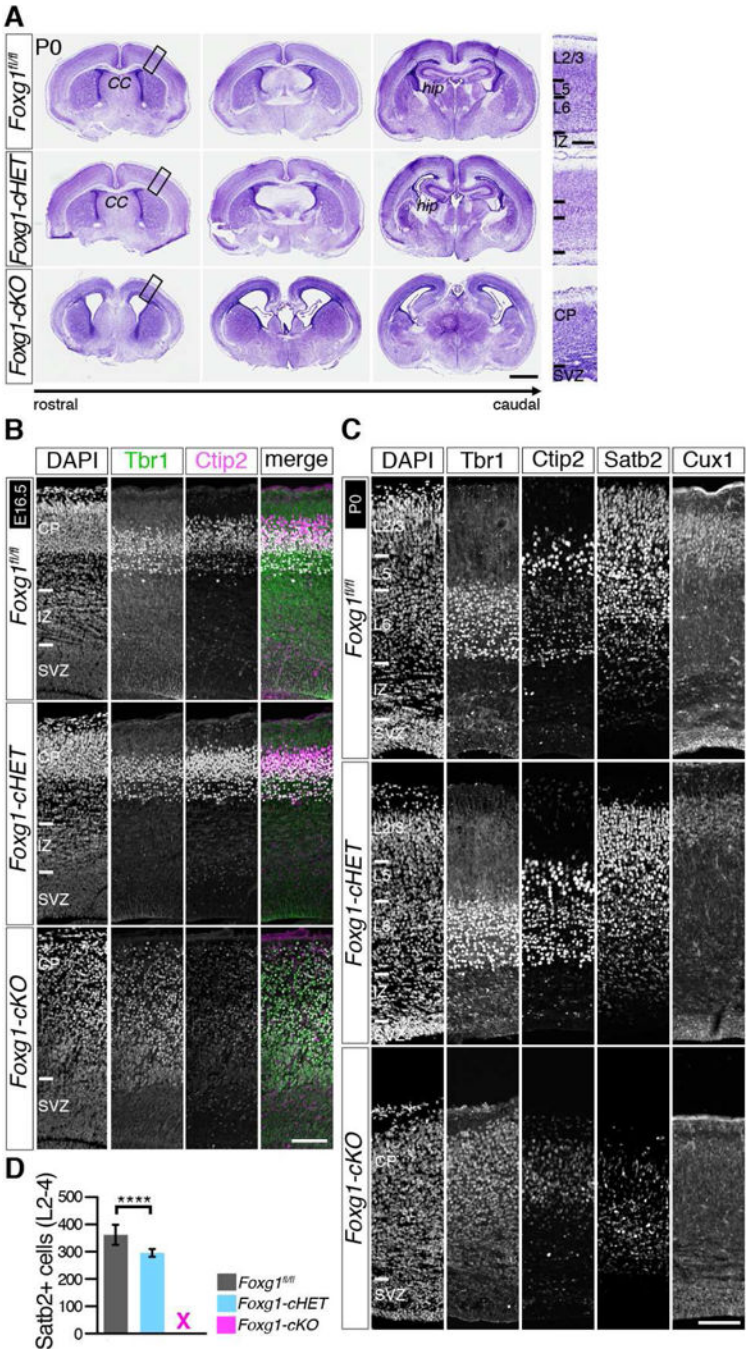

Figure 1. Elimination of Foxg1 in cortical neurons results in defects in the formation of cortical layers and corpus callosum.

(A) *Left*. Cresyl Violet staining of coronal sections of P0 brains of indicated genotypes. *CC*, Corpus Callosum; *hip*, hippocampus. Scale bar, 1mm. *Right*. Magnification of cortical areas as represented on the left by *black insets.* Scale bar, 100μm. (B,C) Immunohistochemical analysis in E16.5 (B) and P0 (C) cortices. Scale bar, 100μm. (D) Quantification analysis of $Satb2^{+}$ cells in P0 cortices. ****, $p<0.0001$. Unpaired *t*-test, $t_{(13)}=5.906$. $n=3$ brains/genotype, 4 slices/brain. Error bars show S.D. See also Figure S1 and S2A–E.

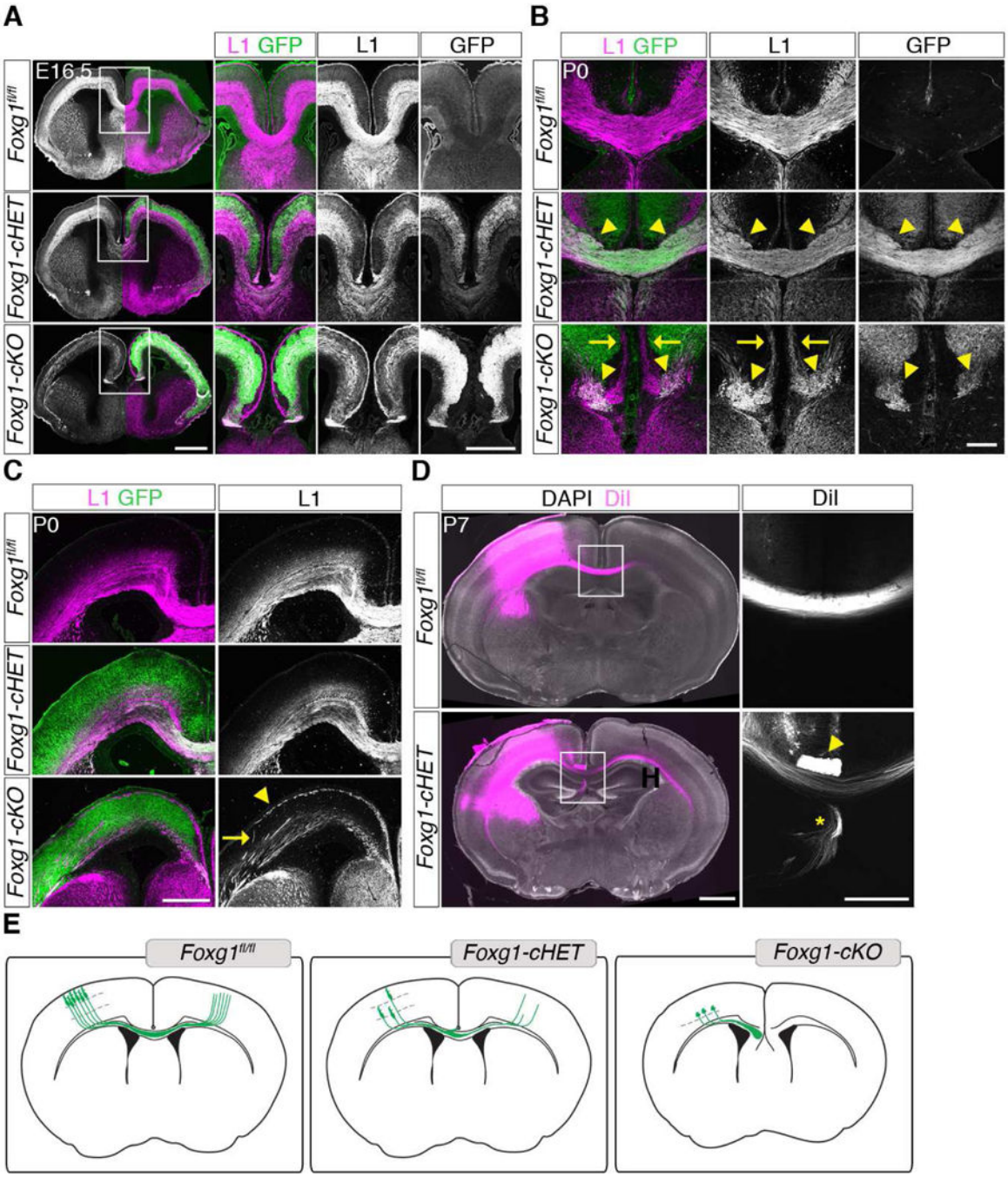

Figure 2. *Foxg1*-deficient brains show severe defects in callosal projections.

(A) *Left.* Immunohistochemical analysis in E16.5 brains of indicated genotypes. GFP staining depicts cortical neurons in which *Foxg1* is deleted by *NEX-Cre.* Scale bar, 500μm. *White boxed areas* highlight the corpus callosum represented in insets on the *right.* Scale bar, 500μm. **(B,C)** Immunohistochemical analyses in P0 brains. (B) Corpus callosum structure. *Arrowheads*, stalled $GFP^+/L1^+$ callosal axons at the midline; *Arrows,* ectopic GFP-negative $L1^+$ axons from subcortical neurons close to the pial surface observed only in *Foxg1-cKO* cortices. Scale bar, 500μm. (C) In *Foxg1-cKO* mice, GFPnegative $L1^+$

thalamocortical axons were misrouted and invaded the cortical plate (*arrow*) and formed the ectopic axon bundle close to the pial surface (*arrowhead*). Scale bar, 500μm. **(D)** Callosal axon projection pattern monitored by DiI, which was injected in somatosensory area of one hemisphere and diffused via callosal axons to the contralateral hemisphere, in P7 *Foxg1* $^{fi/fi}$ or *Foxg1-cHET* brains. Higher magnification of the midline area is shown on the *right*. Scale bar, 1mm (*Left*) or 500μm (*Right*). In *Foxg1-cHET* mice, some callosal axons formed Probst bundles (*arrowheads*) or misprojected towards the septum (*arrow*). **(E)** Schematic representation of cortical neuronal migration and callosal axon tract in *Foxg1* $^{fi/fi}$, *Foxg1-cHET* and *Foxg1-cKO* brains. As Foxg1 levels decrease in *Foxg1* mutant cortices, pyramidal neurons migration and callosal axon tract are perturbed. See also Figure S2G–I.

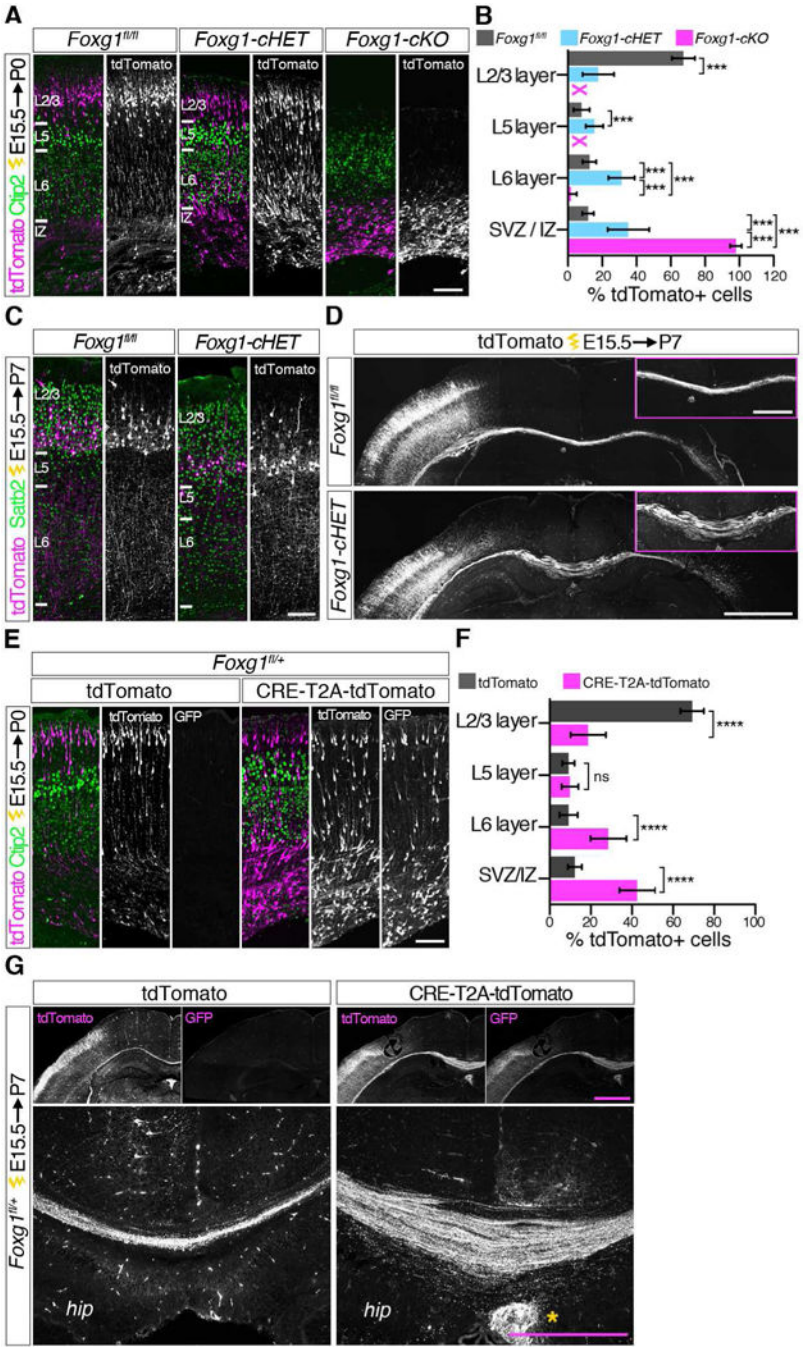

Figure 3. Foxg1 plays a role in directing laminar position and callosal projection of upper layer neurons.

(A-D) Analyses of tdTomato^{+} neuronal migration and axon projection in *Foxg1* $^{fi/fi}$, *Foxg1cHET* and *Foxg1-cKO* brains electroporated at E15.5 and harvested at P0 (A,B) or P7 (C,D). Scale bar, 100μm (A,C). (B) Quantification of the percentage of tdTomato^{+} cells in the area of 750μm x 250μm. One-way ANOVA followed by Tukey *post hoc* test. n=3 *Foxg1* $^{fi/fi}$ (26 slices); n=7 *Foxg1-cHET* (52 slices); n=4 *Foxg1-cKO* (36 slices). ***, p<0.001. SVZ/IZ, $F_{(2,111)}$=896.4; L6, $F_{(2,111)}$=289; L5, $F_{(2,111)}$=153; L2/3, $F_{(2,111)}$=737.2. Error bars show S.D. (D) Midline crossing of tdTomato^{+} neuronal axons. Scale bar, 1mm. *Magenta*

boxes, higher magnification of the midline area. Scale bar, 500μm (main image) or 500μm (inset). **(E-G)** Analyses of tdTomato^{+} neuronal migration and callosal axon projection in *Foxg1*$^{fl/+}$ brains electroporated with tdTomato or CRE-T2A-tdTomato at E15.5 and harvested at P0 (E,F) or P7 (G). Scale bar, 100μm (E). (F) Quantification of the percentage of tdTomato^{+} cells in the area of 750μm x 250μm. ****, $p<0.0001$; *ns*, not significant. Unpaired *t*-test, SVZ/IZ, $t_{(38)}=16.36$; L6, $t_{(41)}=9.747$; L5, $p=0.5221$. $n=3$ brains/condition, 16 slices tdTomato, 28 slices CRE-2A-tdTomato. Error bars show S.D. (G) Callosal axons of tdTomato^{+}GFP^{+} *Foxg1-HET* neurons become defasiculated. Top panels, electroporated neurons expressing tdTomato. GFP is expressed only after CRE-mediated *Foxg1* deletion. Bottom panels, callosal axons crossing the midline. Scale bar, 1mm (top) or 500μm (bottom). (G). *hip*, hippocampus. *star*, electroporated cells in the hippocampus. See also Figure S3.

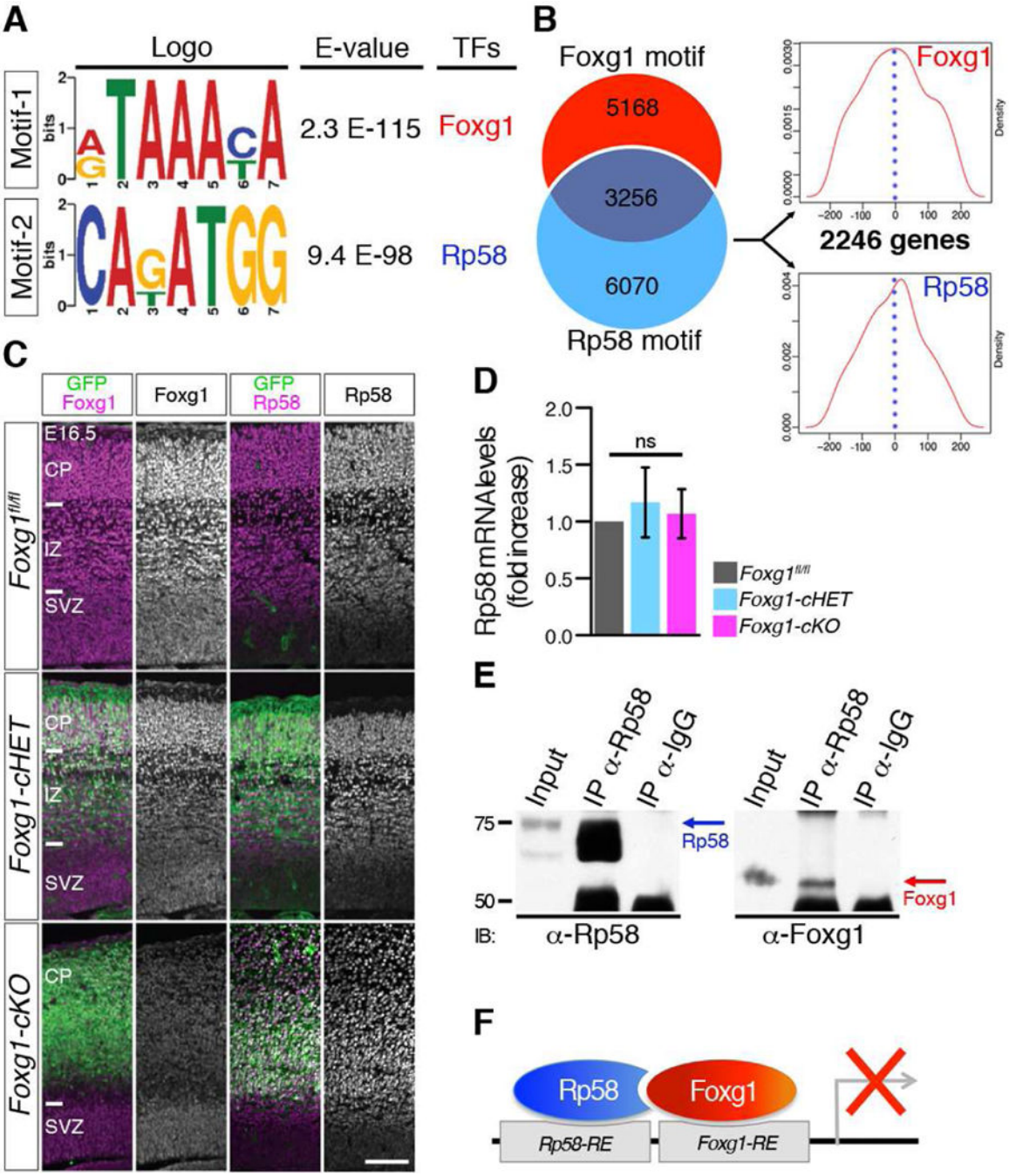

Figure 4. Foxg1 forms a complex with Rp58 to control a subset of Foxg1 target genes in cortical neurons.

(A) Motif analyses of Foxg1-bound ChIPseq peaks revealed that Foxg1- and Rp58-sites are highly enriched in Foxg1-target genomic loci. E-value for each motif was reported by the MEME program. See also Table S1 for the list of peaks. **(B)** Identification of putative genomic target loci and target genes of the Foxg1-Rp58 complex. 3256 Foxg1-bound ChIPseq peaks were identified based on the presence of both Foxg1 and Rp58 motifs within 200 base pair (bp) from the summit of the peak. 5168 ChIPseq peaks contained Foxg1 motif

but no Rp58 motif, whereas 6070 ChIPseq peaks possessed Rp58 motif without Foxg1 motif. The graphs visualize a relative position of Foxg1 and Rp58 motifs within 3256 ChIPseq peaks possessing both Foxg1 and Rp58 motifs. The *x*-axis in the graphs shows −/+300 bp position from the peak summit indicated as 0 on the *x*-axis and blue dotted lines. 3256 ChIPseq peaks were annotated to 2246 target genes (see also Table S2 for the list of peaks and genes). **(C)** Immunohistochemical analyses in E16.5 cortices. Scale bar, 100μm. See also Figure S4A. **(D)** qPCR analysis of Rp58 mRNA levels in E16.5 cortices. *ns*, not significant (one-way ANOVA followed by Tukey *post hoc* test, $F_{(2,19)}=1.177$, $p=0.3297$). **(E)** Co-immunoprecipitation analyses in E16.5 wildtype cortices. Foxg1 forms a complex with Rp58 *in vivo*. IP, immunoprecipitation; IB, immunoblotting. See also Figure S4B. **(F)** The Foxg1-Rp58 complex directly binds and represses its target genes. *Rp58-RE*, Rp58-response element; *Foxg1-RE*, Foxg1-response element.

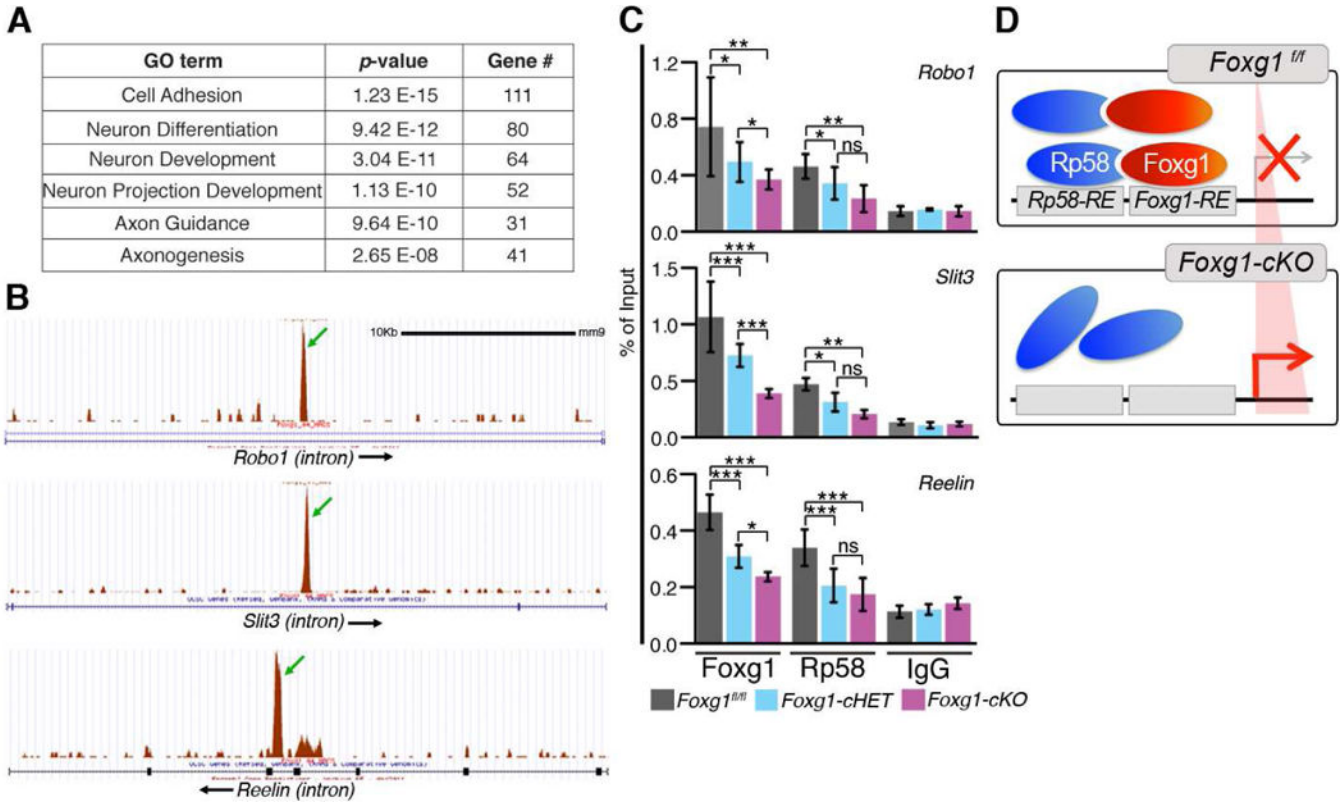

Figure 5. Foxg1-Rp58 targets proneural, neuron migration, and axon guidance genes.

(A) Gene ontology (GO) analyses of 2246 Foxg1-Rp58 target genes. 2246 genes were selected based on their association with 3256 Foxg1-bound ChIPseq peaks containing both Foxg1 and Rp58 motifs. See also Table S3. **(B)** Genome browser view of Foxg1 ChIPseq data for *Robo1, Slit3*, and *Reelin*. Arrows indicate Foxg1-bound peaks tested by independent ChIP analyses in (C). **(C)** ChIP-qPCR analyses in E16.5 cortices. *y*-axis, the percentage of input. *ns*, not significant; *, $p<0.05$; **, $p<0.01$; ***, $p<0.001$; ****, $p<0.0001$. *n*=duplicate of 3 independent experiments. One-way ANOVA followed by Tukey *post hoc* test: *Robo1*, $F(8,45)=13.16$; *Slit3*, $F(8,45)=46.15$; *Reelin*, $F(8,45)=41.31$. See also Figure S4C,D. **(D)** Schematic representation of Foxg1-Rp58 target gene regulation in *Foxg1 fi/fi* and *Foxg1-cKO* brains. As Foxg1 levels reduce, the recruitment of both Foxg1 and Rp58 to the Foxg1-Rp58 target loci decreases. *Rp58-RE*, Rp58-response element; *Foxg1-RE*, Foxg1-response element.

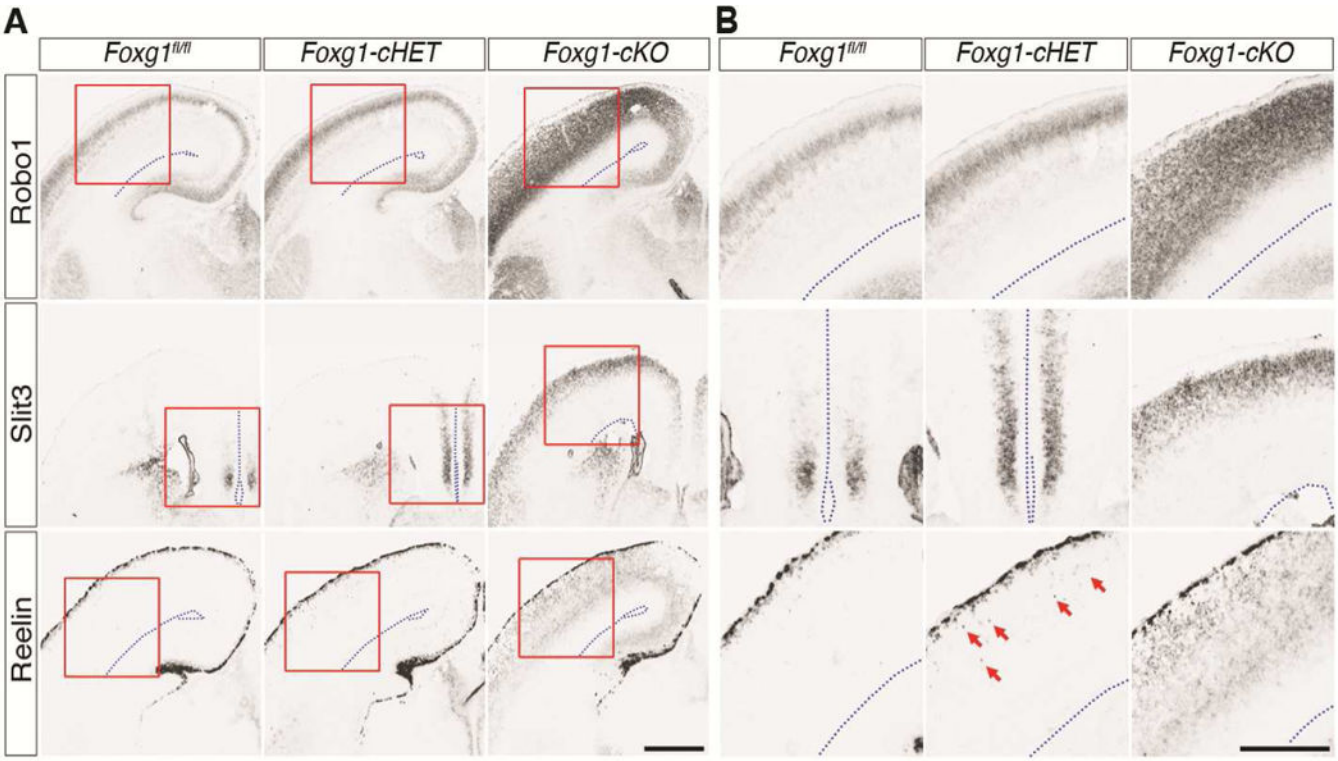

Figure 6. The expression of Robo1, Slit3, and Reelin was derepressed in Foxg1deficient projection neurons in the developing cortex.

ISH analyses of Foxg1-Rp58 target genes in E16.5 brains. (B) shows magnification of cortical area corresponding to the *red boxes* in (A). Scale bar, 1mm (A) or 300μm (B). *Red arrows*, ectopic Reelin^{+} cells in the CP; *Blue dotted lines*, perimeter of brains to mark the ventricle position or midline. See also Figure S5.

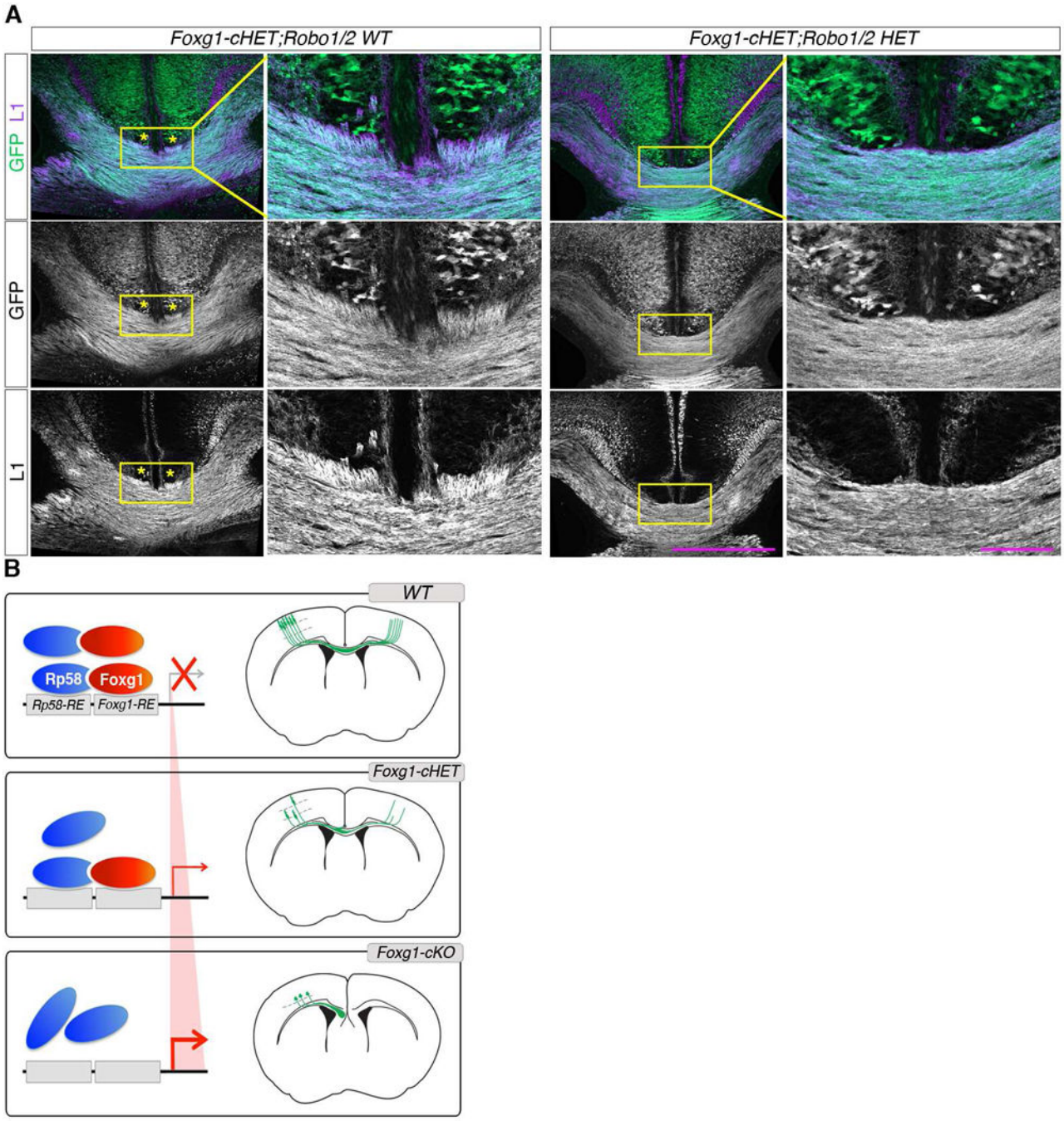

Figure 7. Lowering Robo levels restores callosal axons crossing at the midline.

(A) Immunohistochemical analyses in P0 brains of indicated genotypes. GFP labels axons of cortical neurons in which *Foxg1* is deleted by *NEX-Cre*. *Stars*, stalled $GFP^{+}/L1^{+}$ callosal axons at the midline. *Yellow boxes* highlight midline area magnified on the *right*. Scale bar, 500μm (*left* panels) or 100μm (*right* panels). See also Figure S7. **(B)** Schematic representation of Foxg1-Rp58 target gene regulation and callosal projections in *WT*, *Foxg1-cHET*, and *Foxg1-cKO* cortices. As Foxg1 levels decrease, the Foxg1-Rp58 target genes are

derepressed, and the formation of CPNs and callosal axon tract are perturbed. *RE*, response element.